Science Advances
AAAS

Supplementary Materials for

Instant interfacial self-assembly for homogeneous nanoparticle monolayer enabled conformal "lift-on" thin film technology

Liping Song, Ben Bin Xu, Qian Cheng, Xiaoyuan Wang, Xiaoning Luo, Xue Chen, Tao Chen, Youju Huang*

*Corresponding author. Email: yjhuang@hznu.edu.cn

Published 22 December 2021, *Sci. Adv.* **7**, eabk2852 (2021)
DOI: 10.1126/sciadv.abk2852

The PDF file includes:

Other Supplementary Material for this manuscript includes the following:

Figure S1-S31

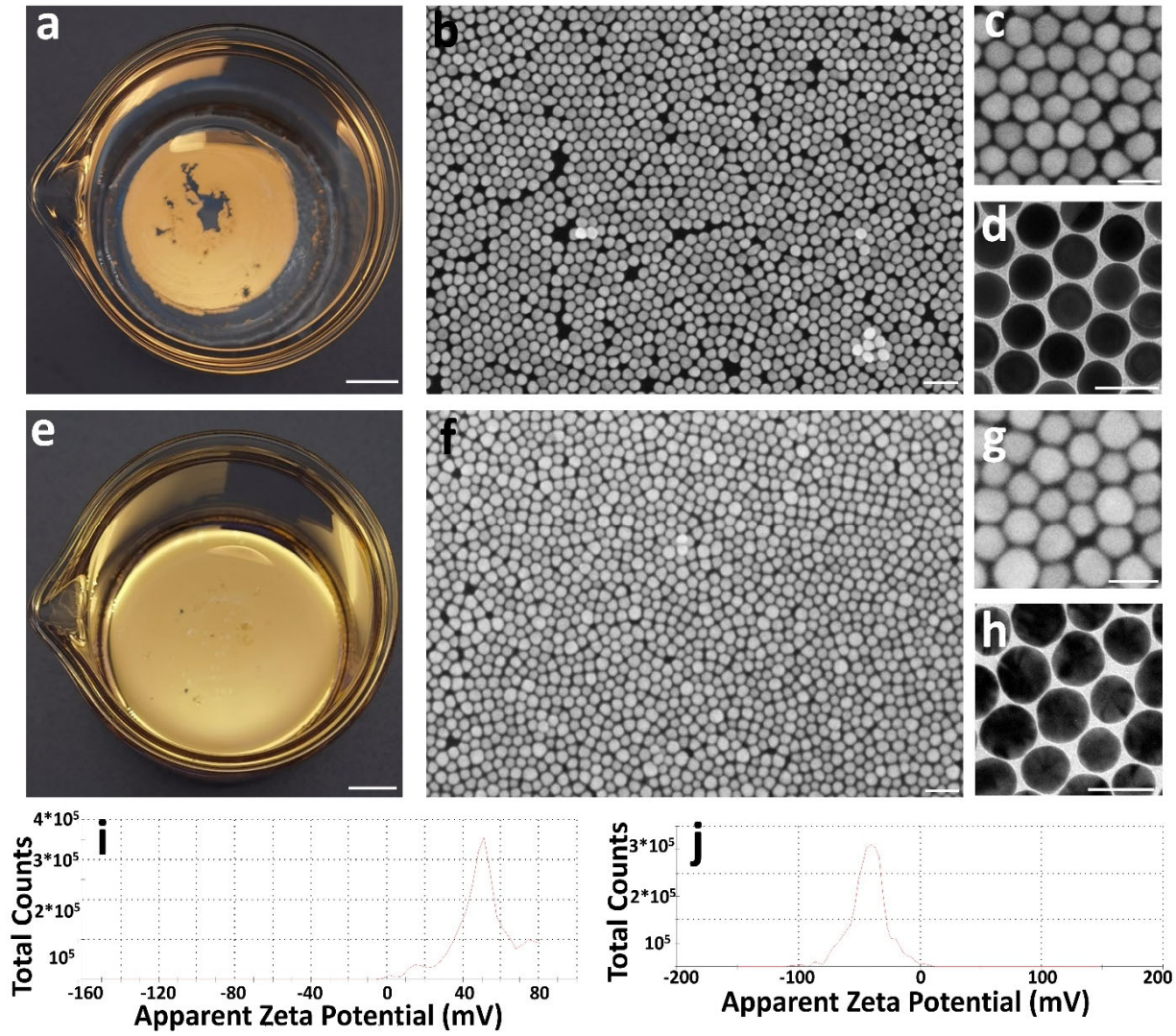

Figure S1. **The PFT induced interfacial assembly of Au NPs with different properties.** The snapshots, SEM and TEM images of 2D Au NPs films formed with different synthesis approaches and surface properties. CTAC-Au NPs (a, b, c, d) and SC-Au NPs (e, f, g, h). (h) Zeta potential distribution histogram of three parallel samples of CTAC-Au NPs (i) and SC-Au NPs (j). The scale bar in a, e is 1 cm, b, f is 100 nm, c, d, g, h is 50 nm, respectively. Photo credit: Liping Song, College of Material, Chemistry and Chemical Engineering, Hangzhou Normal University.

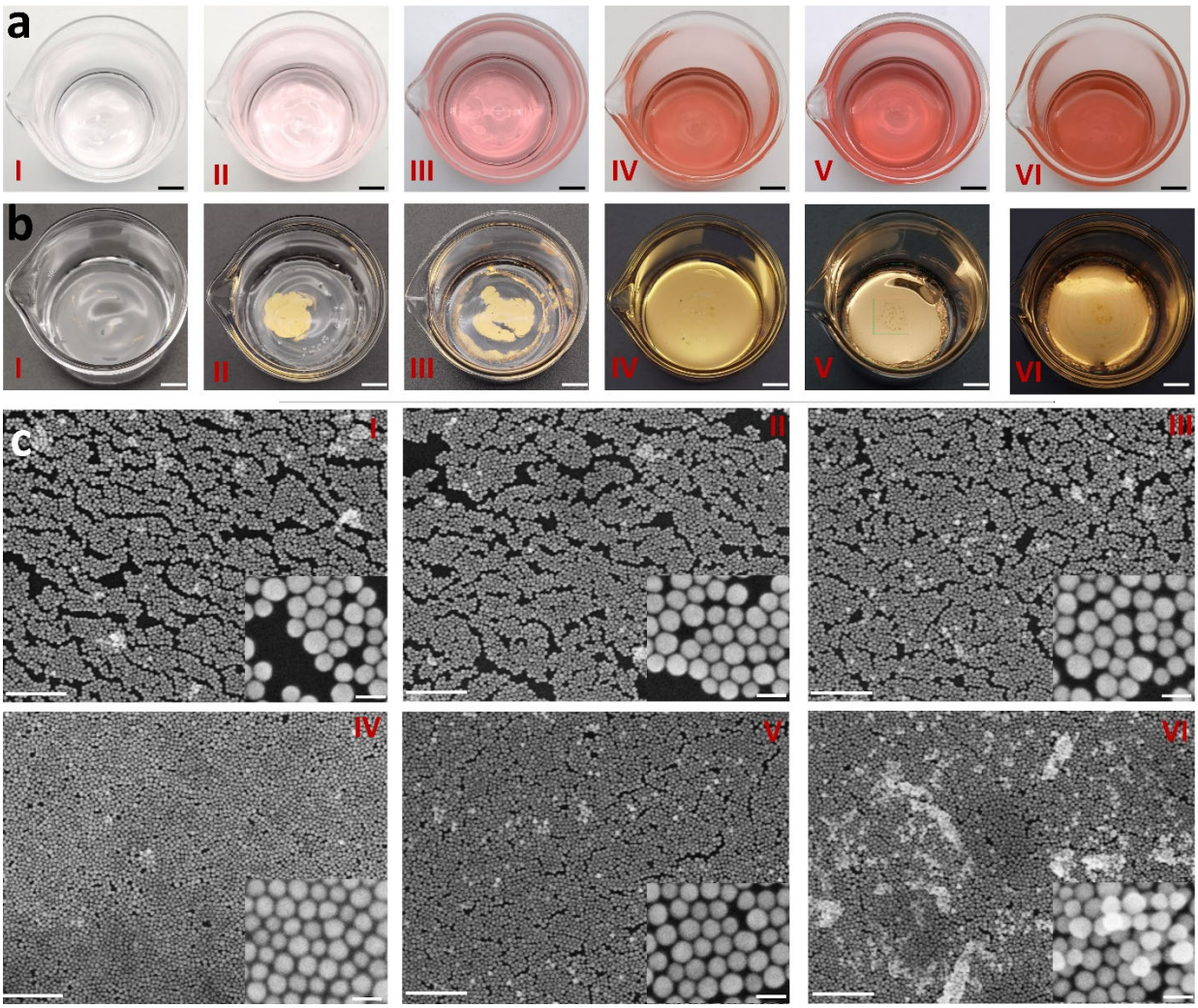

Figure S2. **The influence of the concentration of Au NPs on interfacial assembly.** (a-b) The photographs of Au NPs films with different NPs concentrations in a fixed container. The concentrations from I to VI are 0.49, 4.9, 19.6, 49.0, 78.4 and 98.0 μg/mL, respectively. a: photo of solution before film formation; b: photos after hexane volatilization. (c) the SEM images of 2D Au NPs films with different concentration of Au NPs from I to VI are 0.49, 4.9, 19.6, 49.0, 78.4 and 98.0 μg/mL, respectively. Photo credit: Liping Song, College of Material, Chemistry and Chemical Engineering, Hangzhou Normal University.

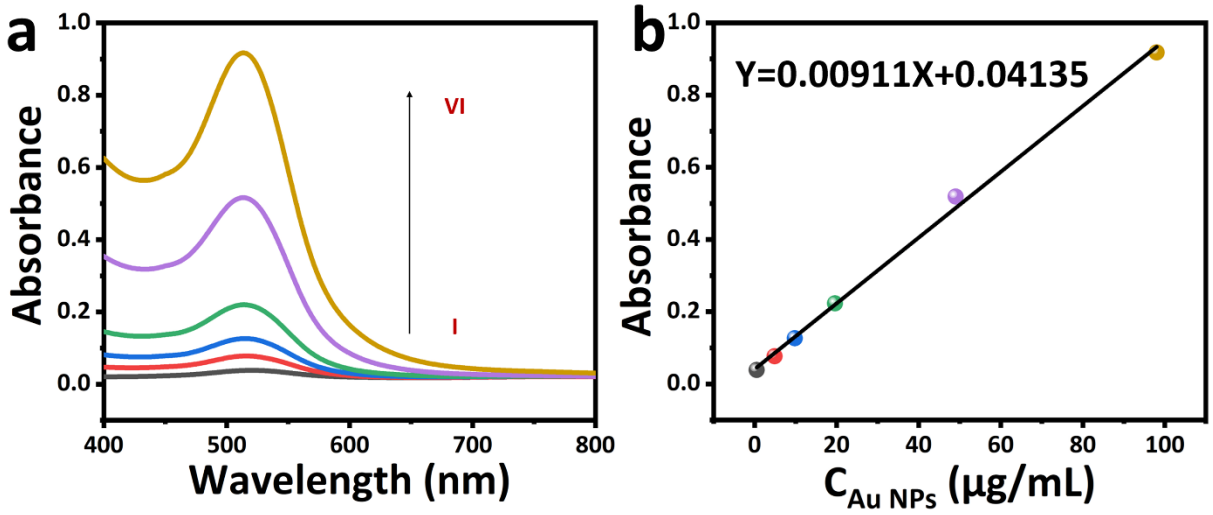

Figure S3. **The linear curve of the UV-vis absorption intensity to the concentration of NPs.** (a) UV-vis absorption spectra of Au NPs standard solutions with different concentrations: from I to VI, the concentrations are 0.49, 4.9, 9.8, 19.6, 49.0 and 96.0 μg/mL; (b) Linear correspondence diagram of absorbance and concentration of Au NPs with different concentrations.

The NPs availability for film formation is calculated as follows:

$$\eta\ (\%) = \frac{A0 - A1}{A0} \times 100$$

in which η is the NPs availability (%), *A0* is the UV-vis absorption intensity of Au NPs stock solution, *A1* is the UV-vis absorption intensity of Au NPs aqueous solution after assembling.

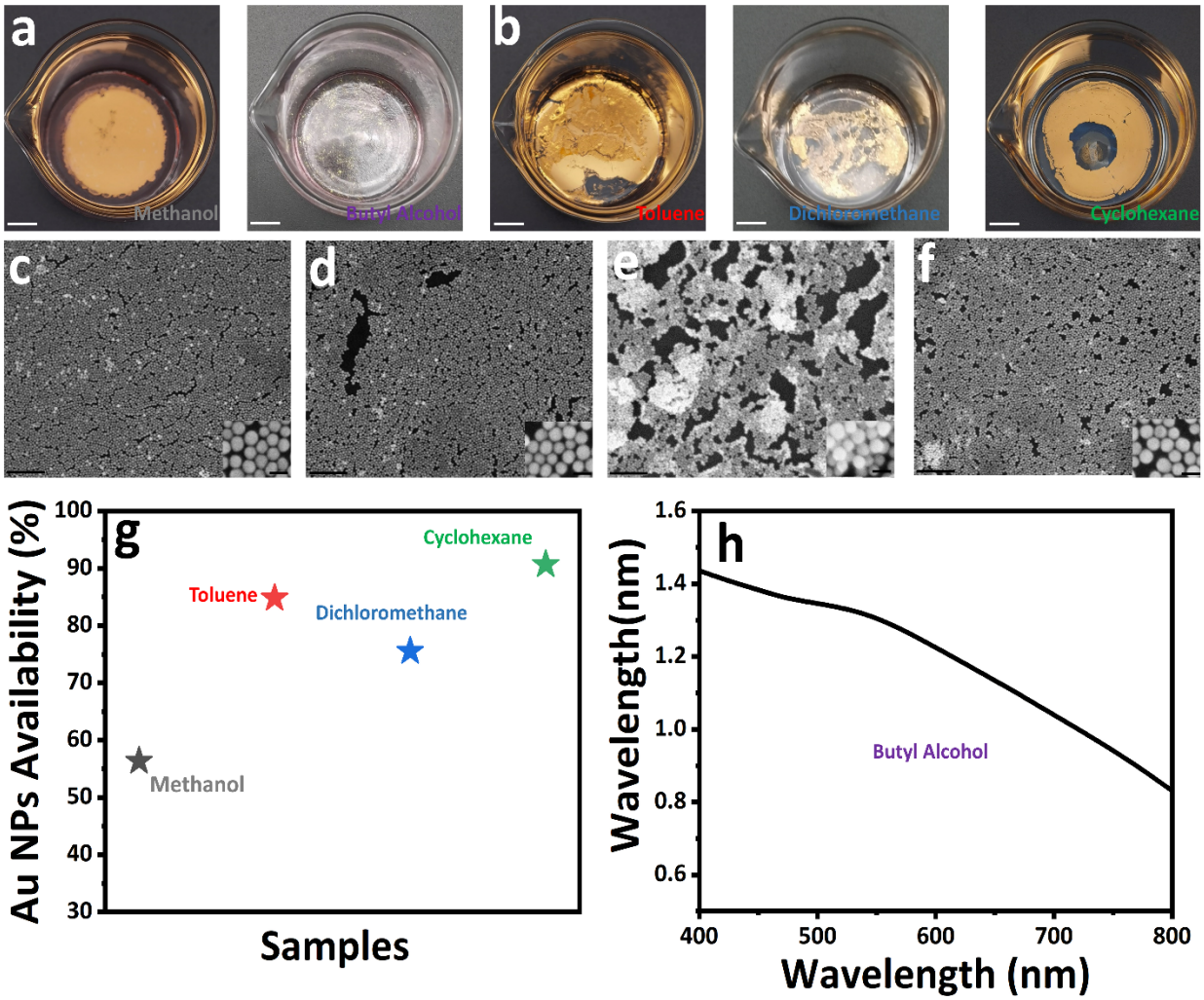

Figure S4. **The influence of solvent types on assembling properties.** The photographs of films formed by replacing ethanol with methanol and butyl alcohol (a), replacing hexane with toluene, dichloromethane as well as cyclohexane (b). The scale bar is 1 cm. The SEM images of Au NPs films obtained with different solvent: (c) methanol, (d) toluene, (e) dichloromethane, (f) cyclohexane. The scale bar is 500 nm and inset is 50 nm, respectively. (g) the Au NPs availability statistic of Au NPs for assembly with different solvent. (h) The wide UV-vis absorption of Au NPs after assembling with butyl alcohol. Photo credit: Liping Song, College of Material, Chemistry and Chemical Engineering, Hangzhou Normal University.

As the oil solvent, four requirements should be meet: (1) completely immiscible with water with low surface tension; (2) incompatible with PFT; (3) relatively small saturated vapor pressure; (4) environment friendly. As the "inducer" solvent, there are also three requirements should be meet to obtain unfirm and density film: (1) miscible with water, hexane and PFT, and the solubility relationship is water>hexane>PFT; (2) low dielectric constant solvent; (3) environment friendly. Although we have conducted the control solvent species experiment, we find there are very few solvents that meet these limitations and hexane and ethanol are more suitable for our interfacial assembly system.

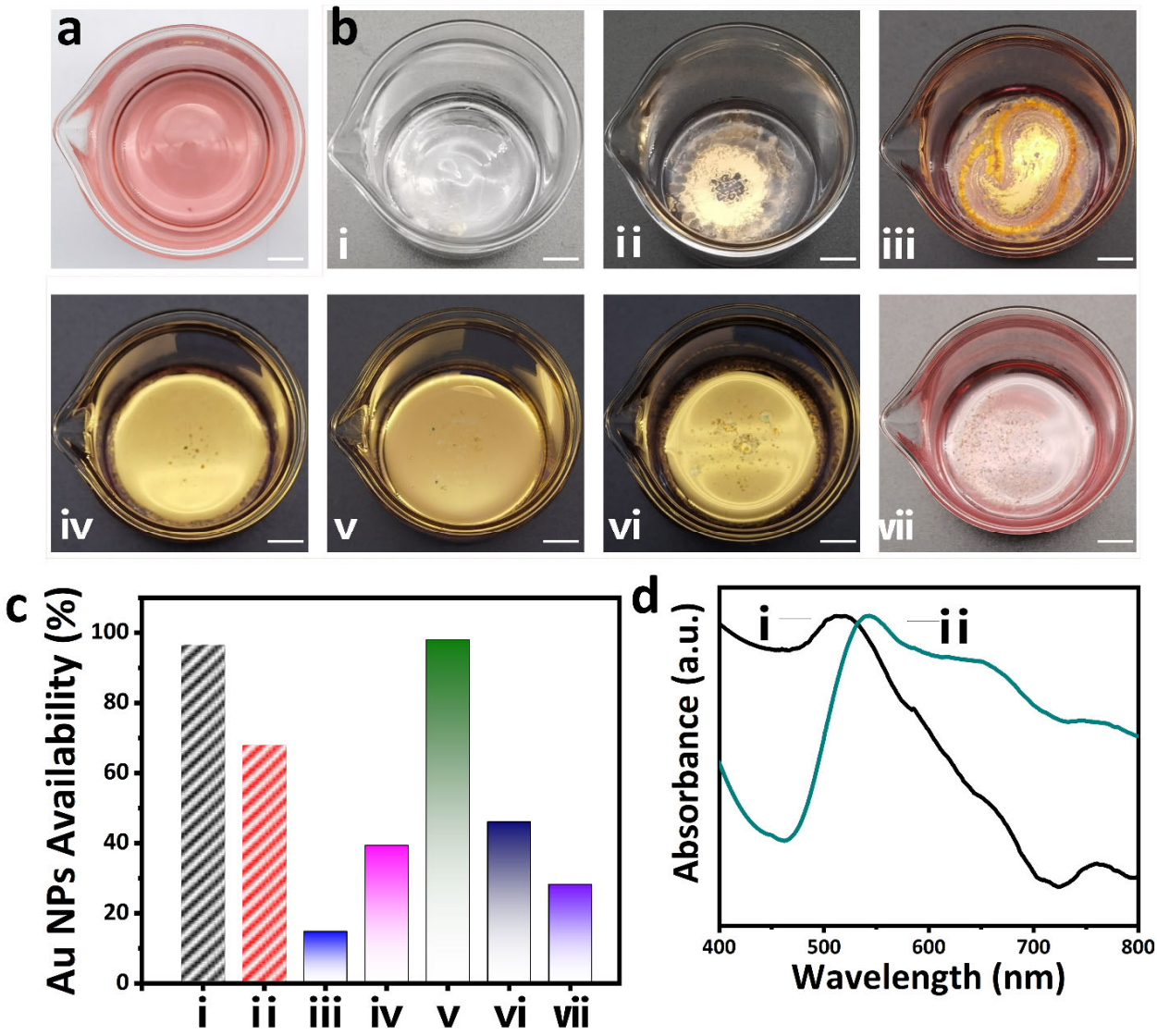

Figure S5. **The influence of V_{hexane}: $V_{ethanol}$ on PFT induced interfacial assembly.** (a) The photograph of Au NPs stock solution used for assembling; (b) The photographs of Au NPs films after assembling with different amounts of hexane and ethanol: (i) Hexane (10 mL); (ii) Hexane: Ethanol=4:1; (iii) Hexane: Ethanol=2:1; (iv) Hexane: Ethanol=1:1; (v) Hexane: Ethanol=1:2; (vi) Hexane: Ethanol=1:4; (vii) Ethanol (10 mL). (c) The histogram of NPs availability for film formation of different amounts of hexane and ethanol. (d) the UV-vis spectra of aqueous solution after film formation: (i) Hexane (10 mL); (ii) Hexane (8 mL): Ethanol (2 mL). Photo credit: Liping Song, College of Material, Chemistry and Chemical Engineering, Hangzhou Normal University.

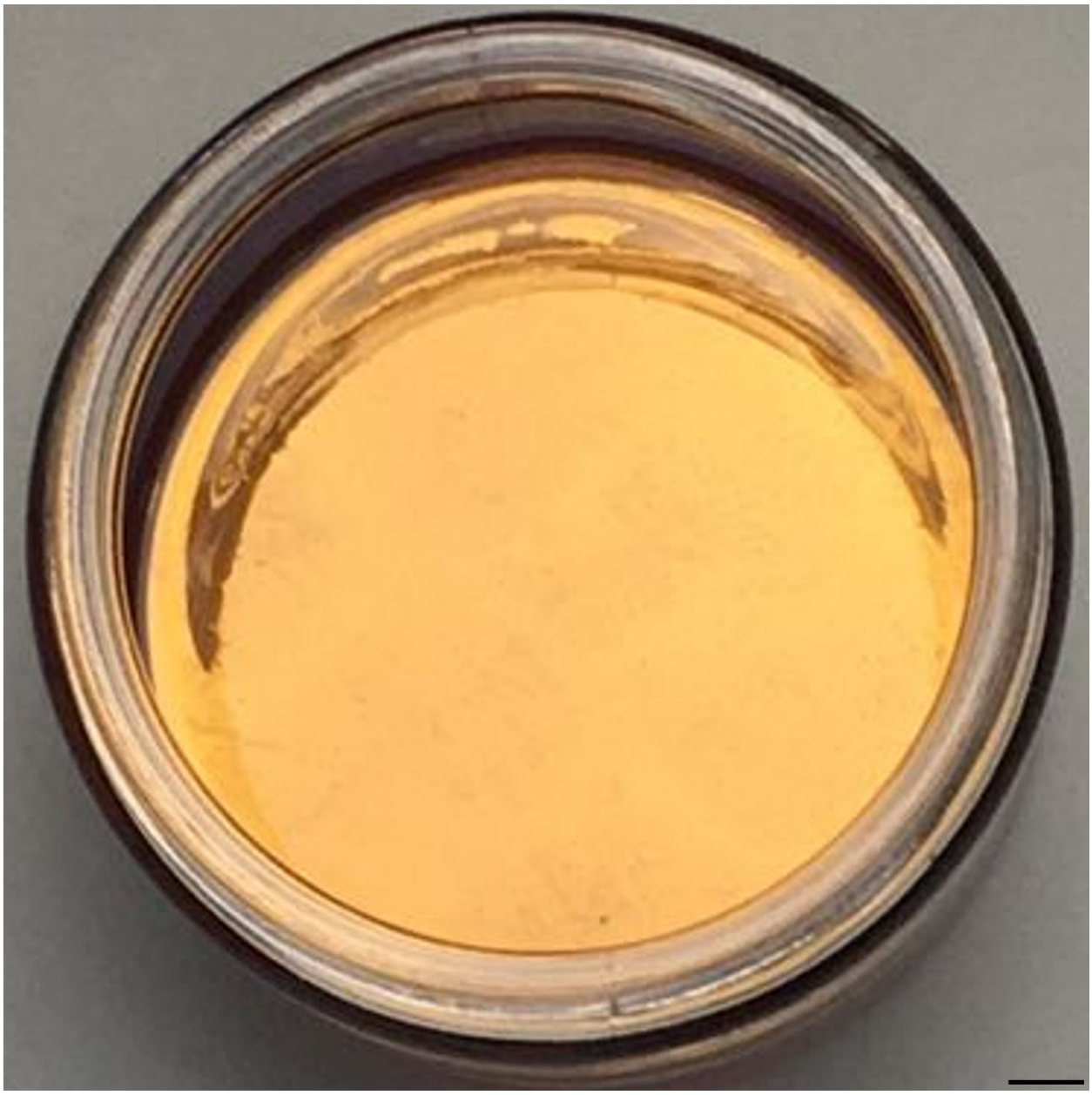

Figure S6. **The photograph of Au NPs assembled film with size up to 4.3-inch wafer.** The photograph of Au NPs assembled film with size up to 4.3-inch wafer. The scale bar is 1 cm. Photo credit: Liping Song, College of Material, Chemistry and Chemical Engineering, Hangzhou Normal University.

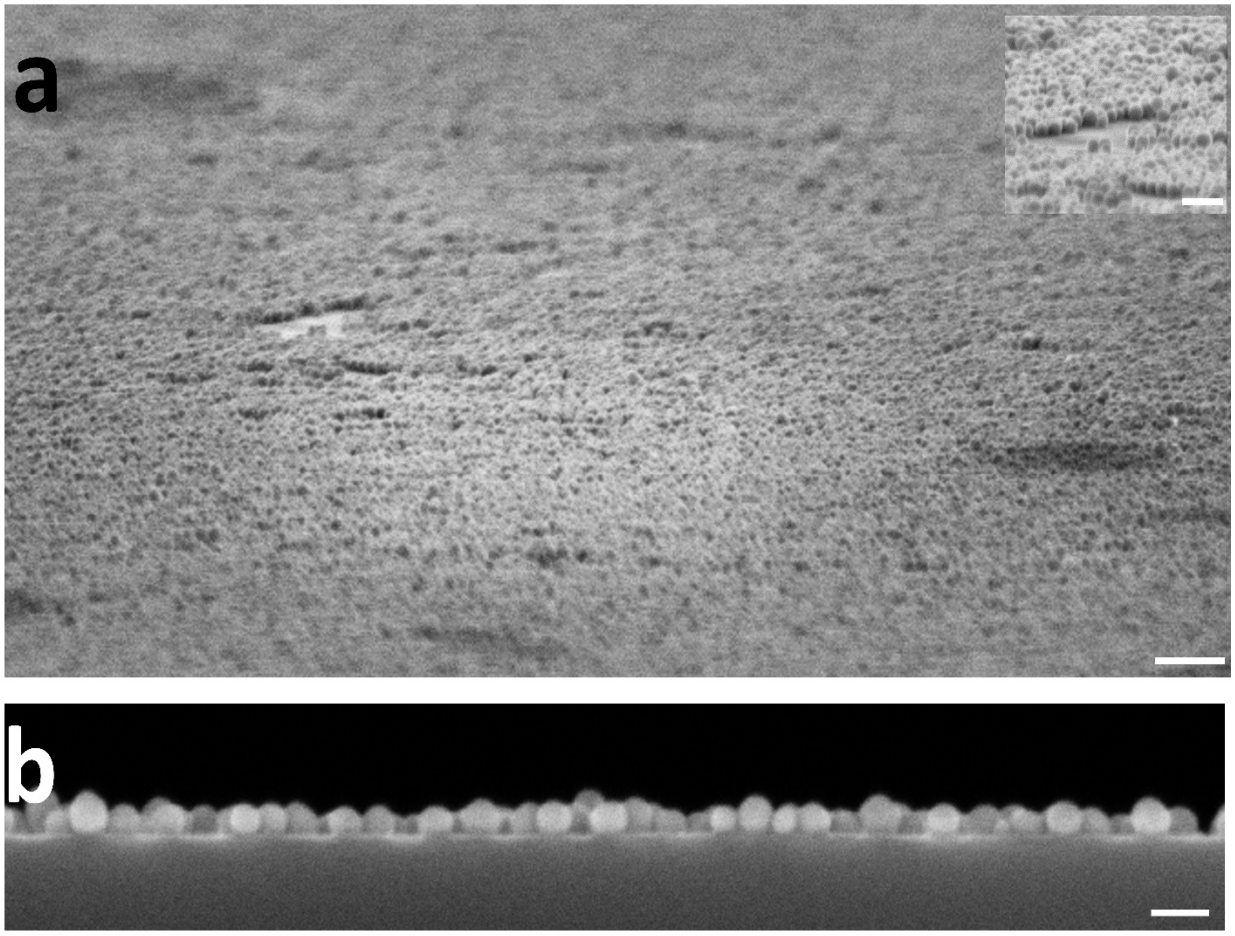

Figure S7. **The SEM cross-sections of Au NPs monolayer films.** The scale bar in a, b and inset pictures is 100 nm and 50 nm, respectively.

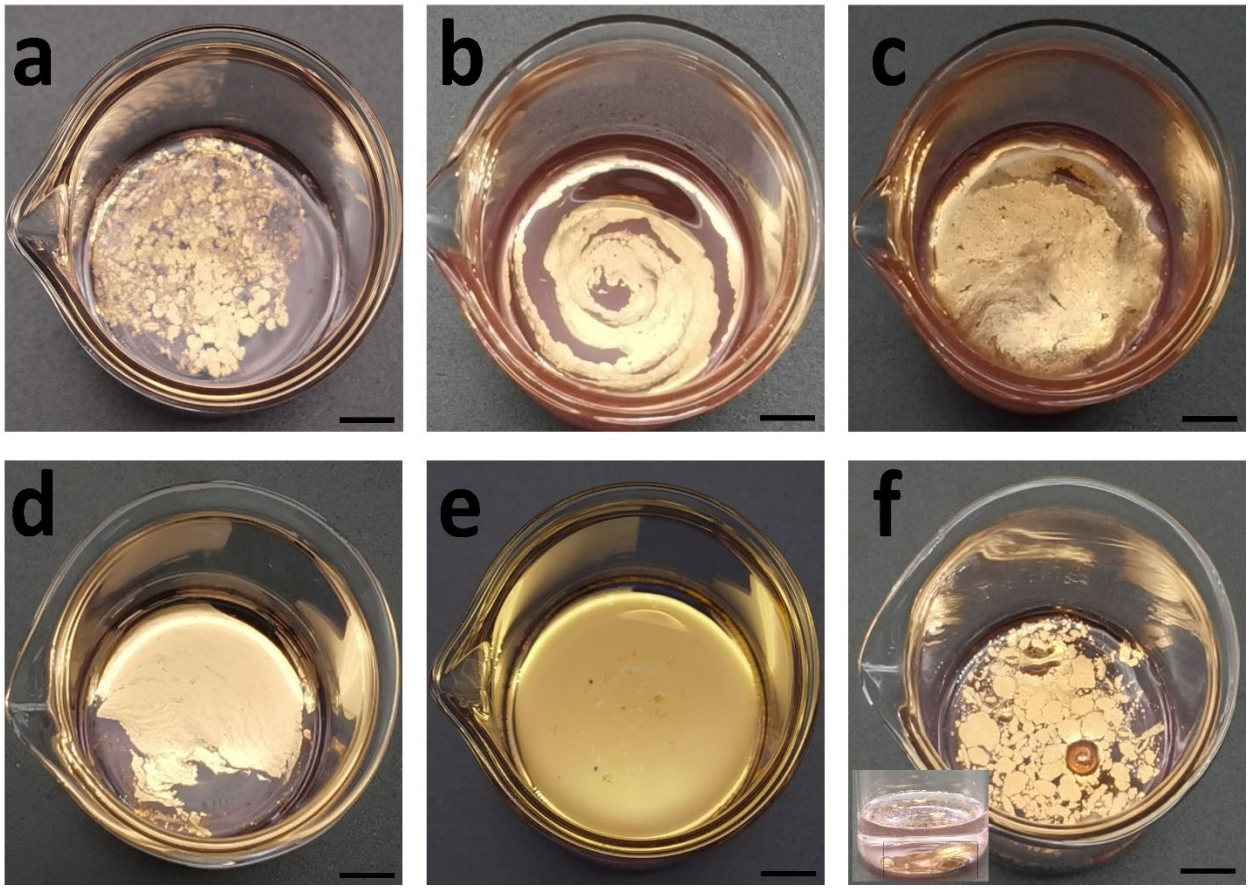

Figure S8. **The influence of PFT concentration on interfacial assembly.** The photographs of Au NPs water dispersion and Au NPs films with different concentration of PFT, the concentration of PFT from (a) to (f) is 100 nM, 20 μM, 100 μM, 1 mM, 10 mM and 100 mM, respectively. The scale bar is 1 cm. Photo credit: Liping Song, College of Material, Chemistry and Chemical Engineering, Hangzhou Normal University.

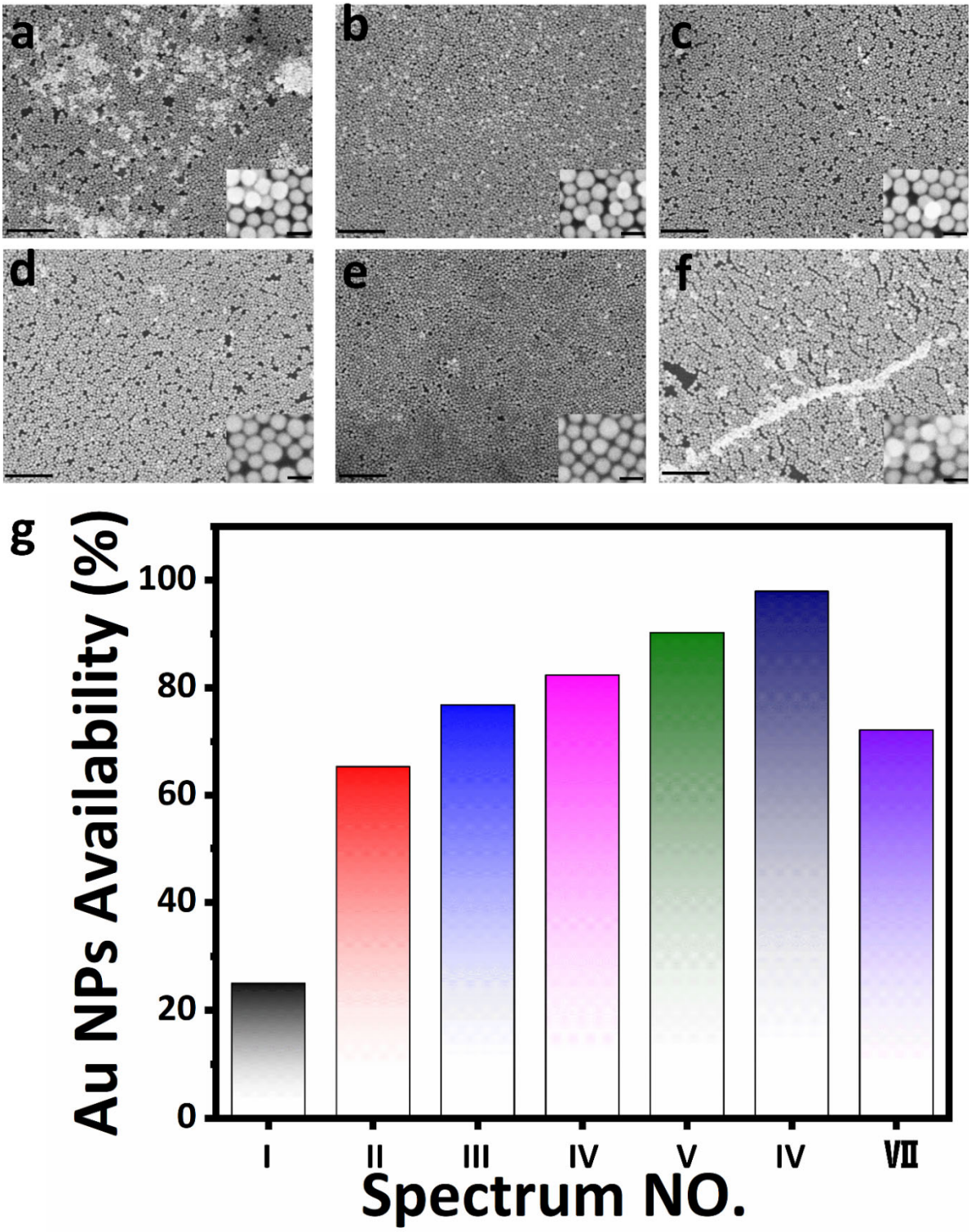

Figure S9. **The SEM images and NPs availability of Au NPs films obtained with different concentration of PFT.** The SEM images of Au NPs assembled with different concentration of PFT, the concentration of PFT from a to f is 100 nM, 20 μM, 100 μM, 1 mM, 10 mM and 100 mM, respectively. The scale bar in a-f and inset pictures are 100 nm and 50 nm, respectively. The Au NPs availability for assembly with different concentration of PFT, from I to VII is 0 nM, 100 nM, 20 μM, 100 μM, 1 mM, 10 mM and 100 mM, respectively. Photo credit: Liping Song, College of Material, Chemistry and Chemical Engineering, Hangzhou Normal University.

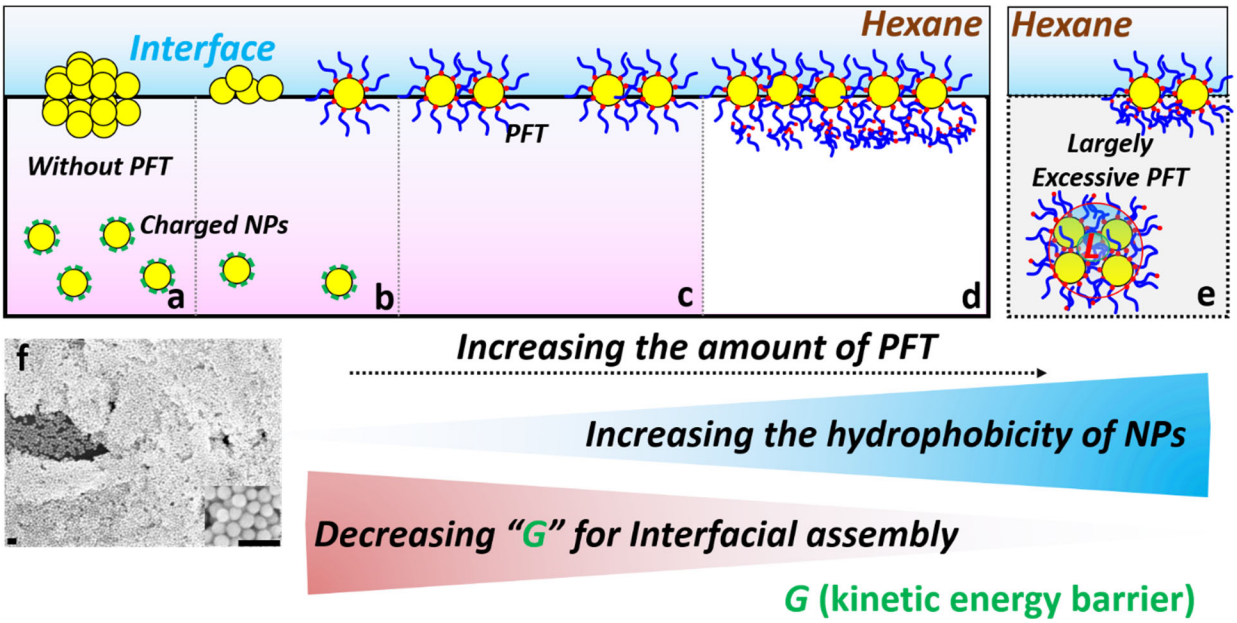

Figure S10. **Schematic illustration of concentration effect of PFT on interfacial assembly structures** (a-d). SEM image of Au NPs film obtained with huge excessive PFT. The scale bar is 100 nm.

As shown in **Figure S10**, aggregations of NPs are likely to appear via interfacial assembly without PFT (a, f). Unlike traditional interfacial assembly achieved by ethanol injecting approach (>30 min) *(15)*, the rapid mixing of ethanol with Au NPs without PFT results in uncontrollable decrease of NPs surface charge, thus lead to poor film uniformity. By increasing the amount of PFT, the aggregates significantly reduced and replaced by uniform NPs monolayers (b, c). This interfacial assembly is tailored by gradually increased hydrophobicity of NPs endowed by PFT. When the PFT amount exceed the critical value for an indefinite volume, it will benefit the process to obtaining uniform film with desired density (d), by strengthening the assembly speed and high hydrophobicity of NPs. When the amount of PFT is significant over the critical value, "metal droplet" seems to be likely to generate at the bottom of the container. Similar to the "metal droplet" reported by others (*51*), the phase separation of excessive PFT ("***L***" in Figure S10) and water account for this phenomenon.

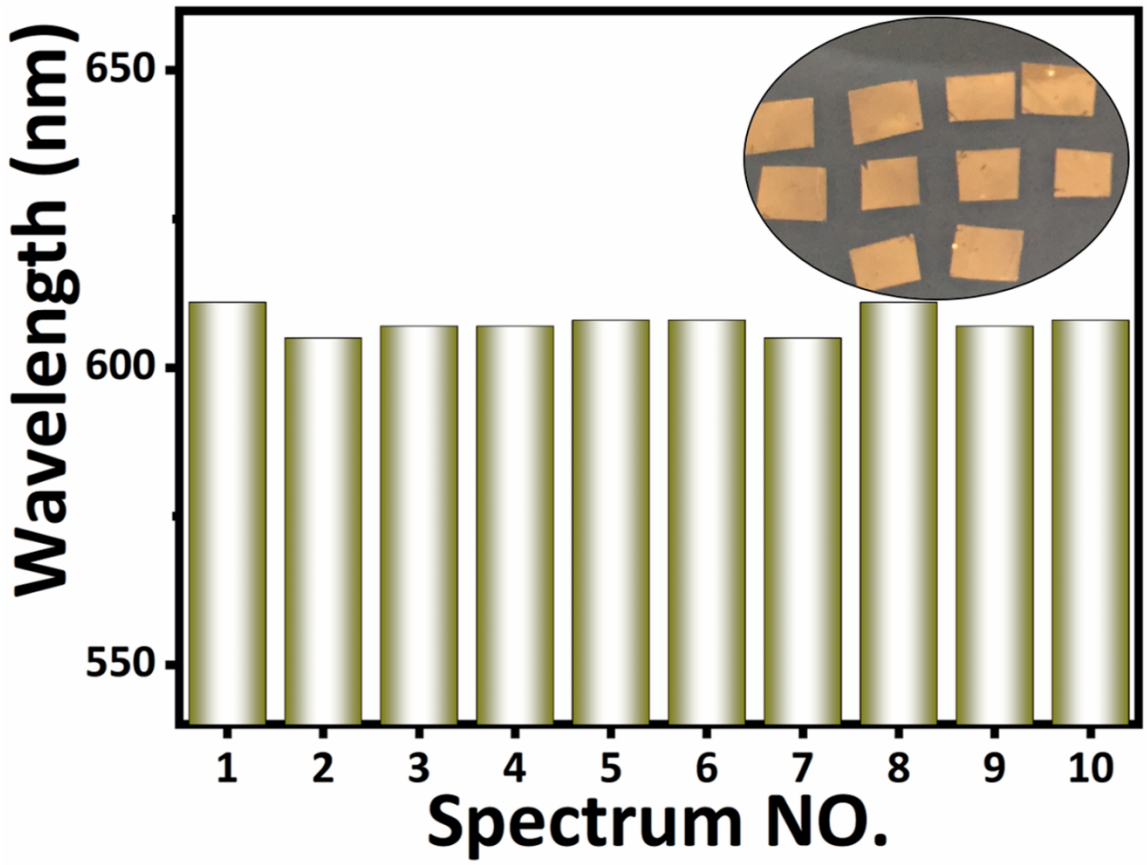

Figure S11. **Intensity distribution of the UV-vis absorption of Au NPs monolayer films.** 10 samples of Au NPs films were selected. Photo credit: Liping Song, College of Material, Chemistry and Chemical Engineering, Hangzhou Normal University.

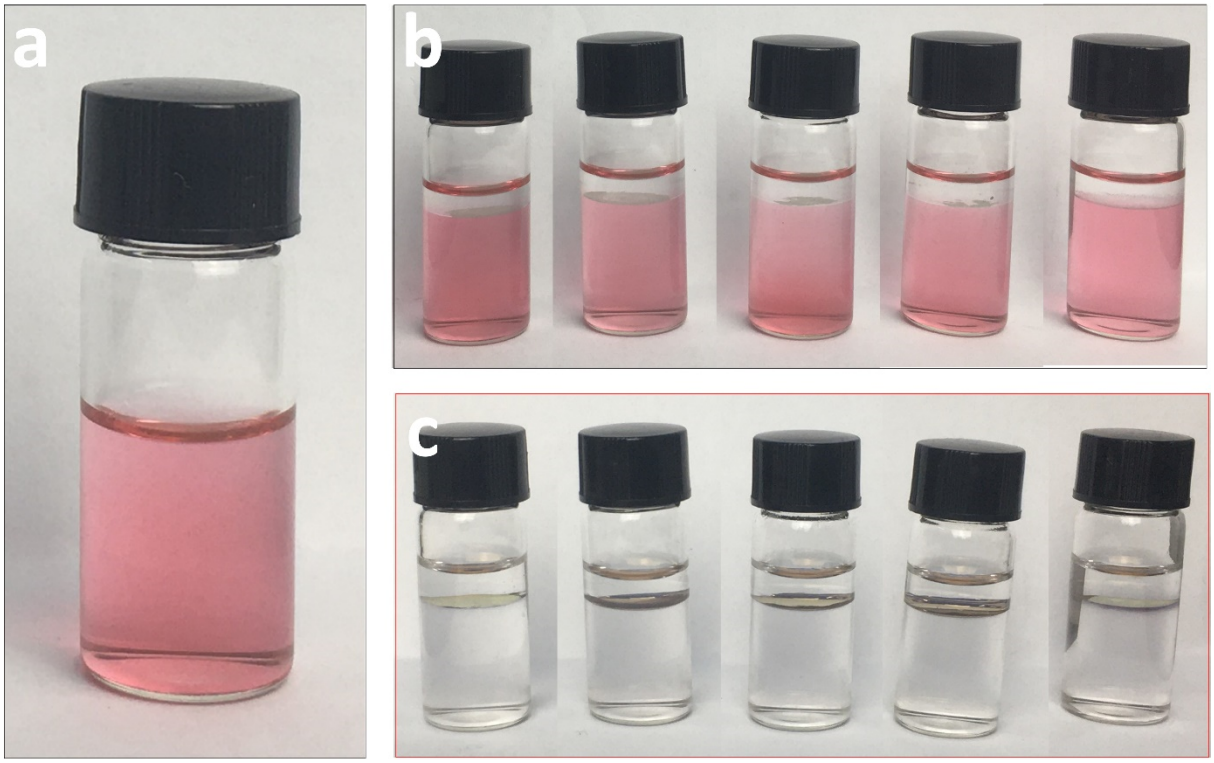

Figure S12. **The outstanding NPs availability of PFT induced interfacial assembly.** The real images of Au NPs stock solution (a), Au NPs solution after assembly without PFT (b) and Au NPs solution after assembly with PFT (c). Photo credit: Liping Song, College of Material, Chemistry and Chemical Engineering, Hangzhou Normal University.

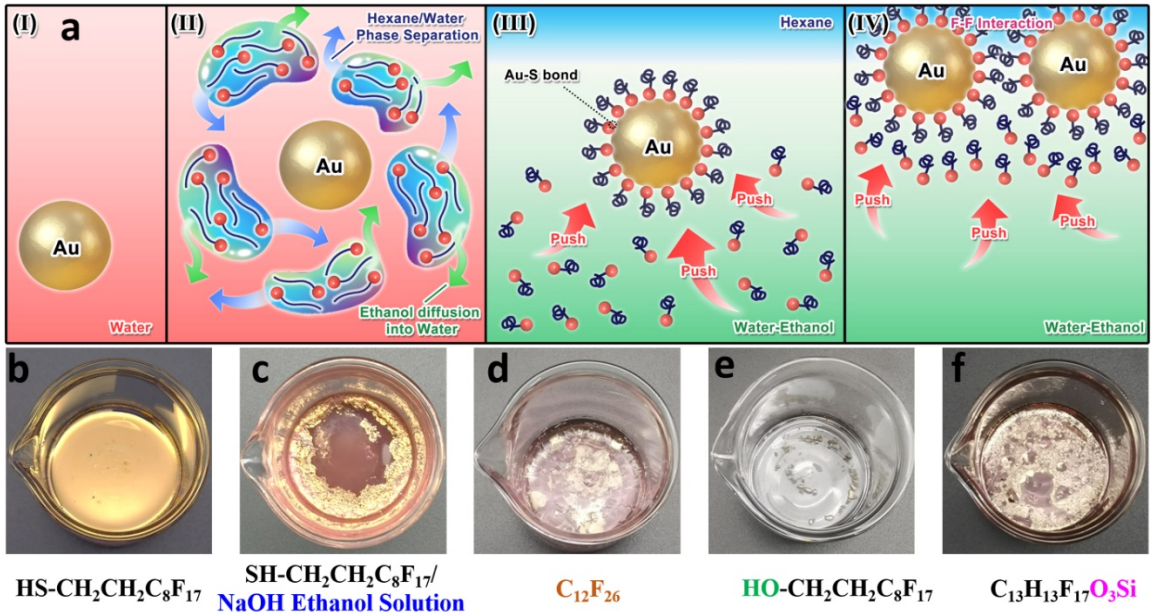

Figure S13. **Schematic diagram of possible assembly procedure and NPs films after assembling with other perfluorinated molecules without sulphydryl groups.** (a) Schematic diagram of possible superfast assembly procedure of Au NPs induced by PFT at water-hexane interface: (I) Au NPs stabilized in aqueous solution; (II) Adding mixture solution of PFT in ethanol/hexane; (III) the interaction between Au NPs and PFT; (IV) The

moving of Au NPs to interface; (b-f) The comparation of Au NPs assemblies obtained by inducing different perfluorinated molecules. Photo credit: Liping Song, College of Material, Chemistry and Chemical Engineering, Hangzhou Normal University.

Some similar perfluorinated molecules to PFT with different functional groups were induced to replace PFT for verifying the key role of PFT and Au-S interaction for assembly. Considering the relatively good solubility of hydrophobic thiol molecules in alkaline ethanol solution, the Au NPs assembly with alkaline PFT mixture solution presented obvious poor performance. More importantly, most of Au NPs can not be utilized for assembly at interface, as shown in **Figure S12c**. This result verified our conjecture that the poor insolubility of PFT in water/ethanol mixture solution play key roles for interfacial assembly. In addition, the poor interfacial performance of other perfluorinated molecules without -SH strongly confirmed the key role of Au-S interaction for assembly, as shown in **Figure S12d-f**.

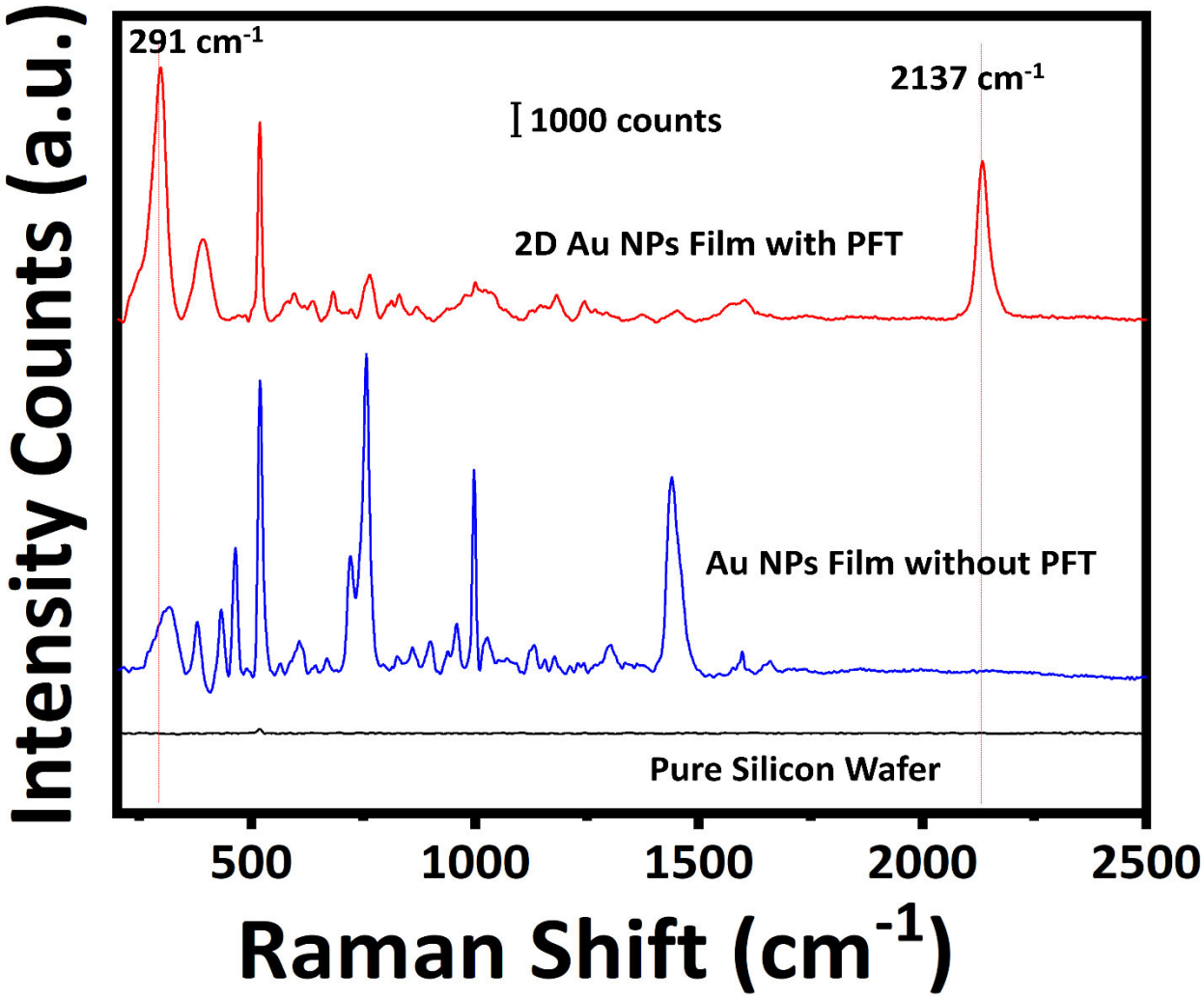

Figure S14. **Raman spectrum of Au NPs films.** Raman spectrum of different samples of pure silicon (curve a), Au NPs film without PFT (curve b) and 2D Au NPs film with PFT (curve c).

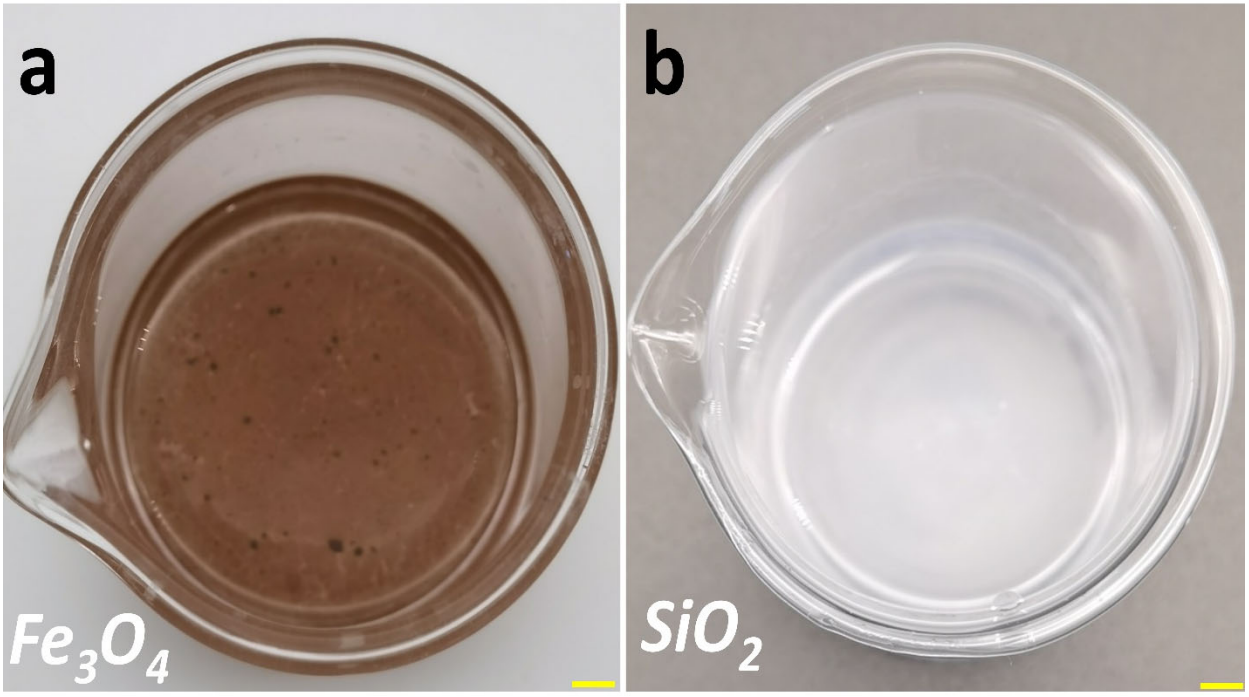

Figure S15. **The photographs of Fe_3O_4 and SiO_2 nanoparticles films assembled at interface.** The scale bar is 1 cm. Photo credit: Liping Song, College of Material, Chemistry and Chemical Engineering, Hangzhou Normal University.

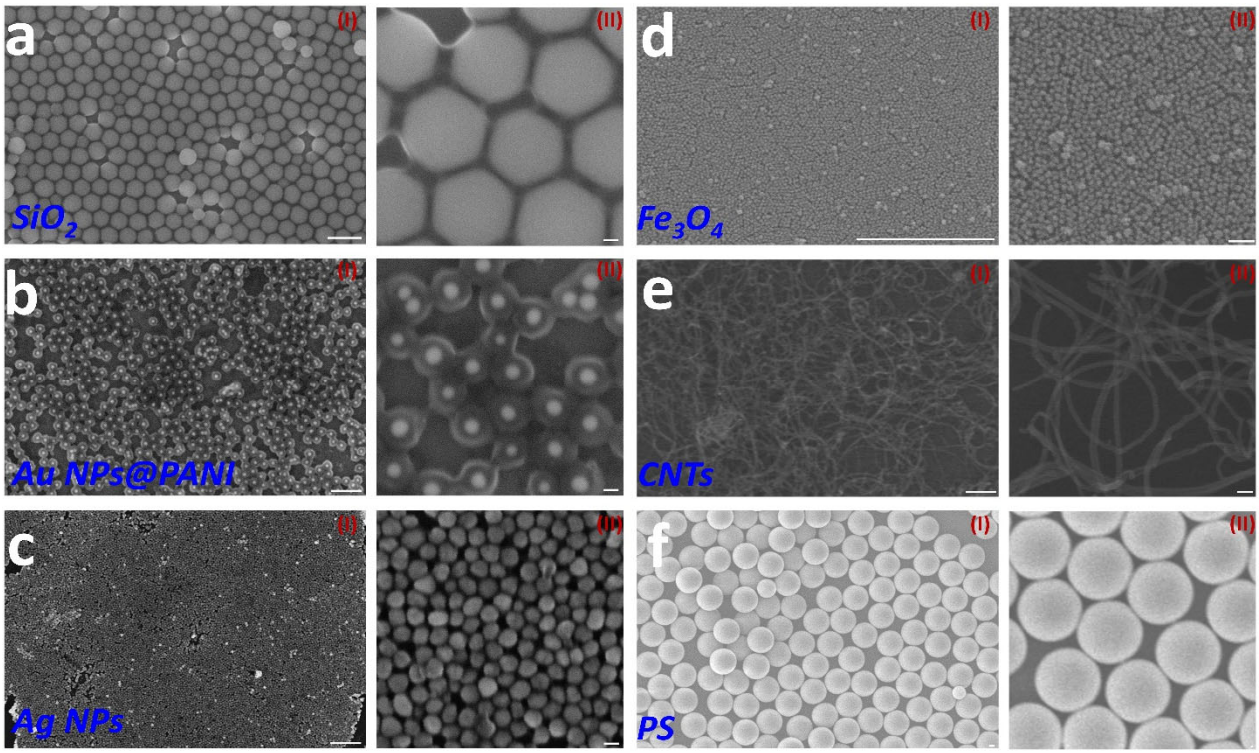

Figure S16. **The SEM images of assemblies of different materials.** The scale bar in (I) and (II) is 500 nm and 50 nm, respectively.

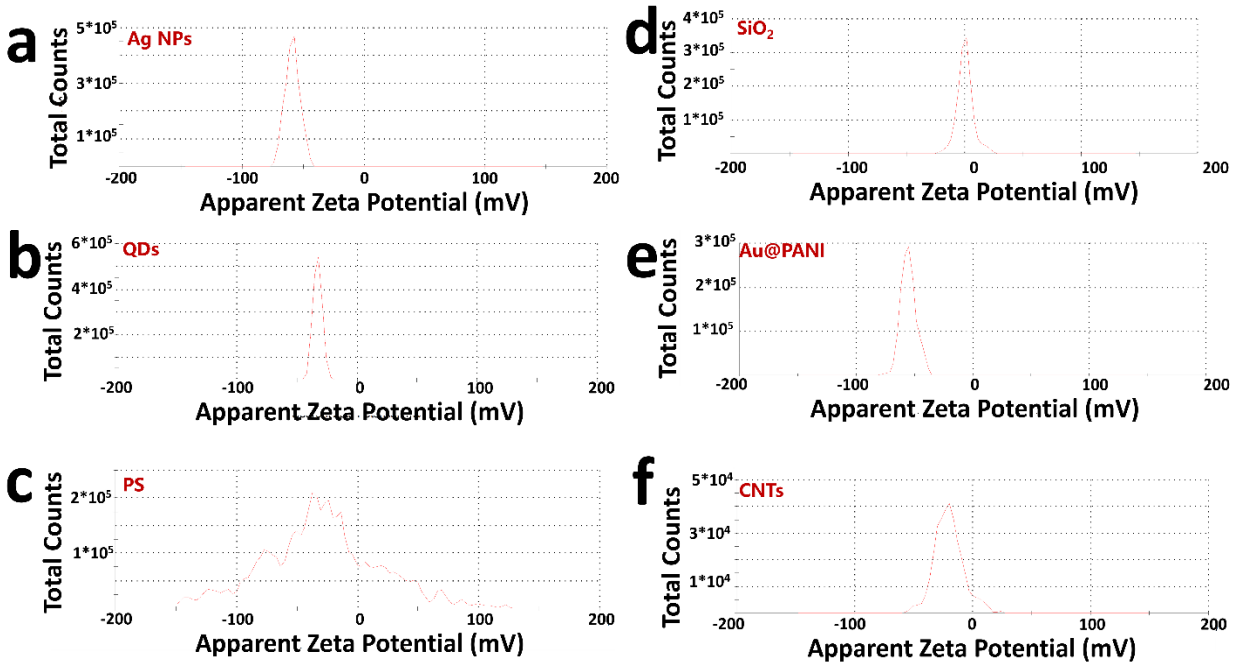

Figure S17. **The surface charge properties of different materials for interfacial assembly.**

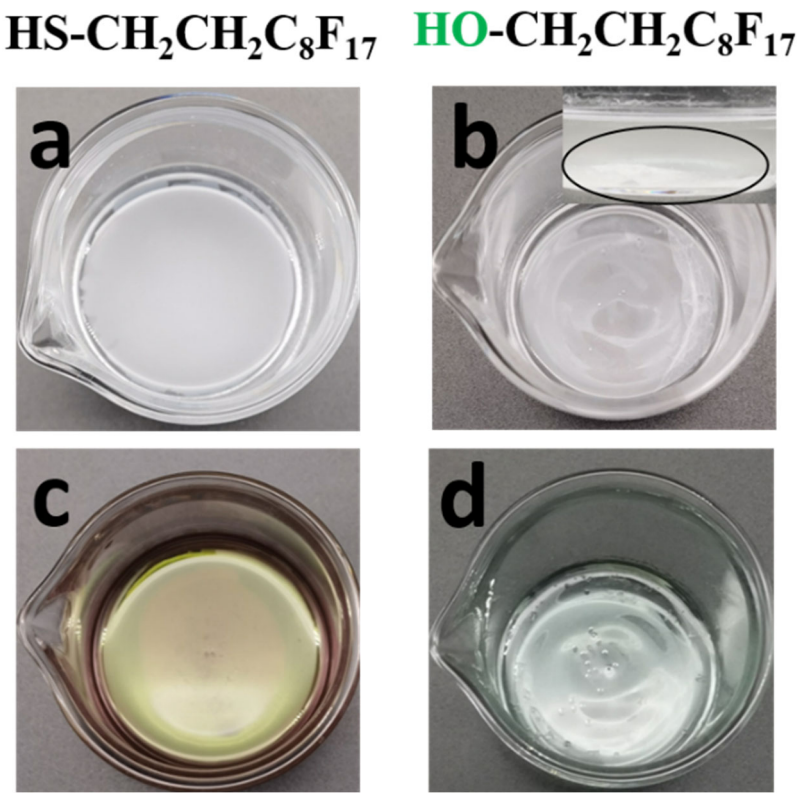

Figure S18. **The photographs of PS and Au NPs@PANI films obtained with different perfluorinated molecules.** (a, c) PFT; (b, d) perfluoro-1-decanol. Photo credit: Liping Song, College of Material, Chemistry and Chemical Engineering, Hangzhou Normal University.

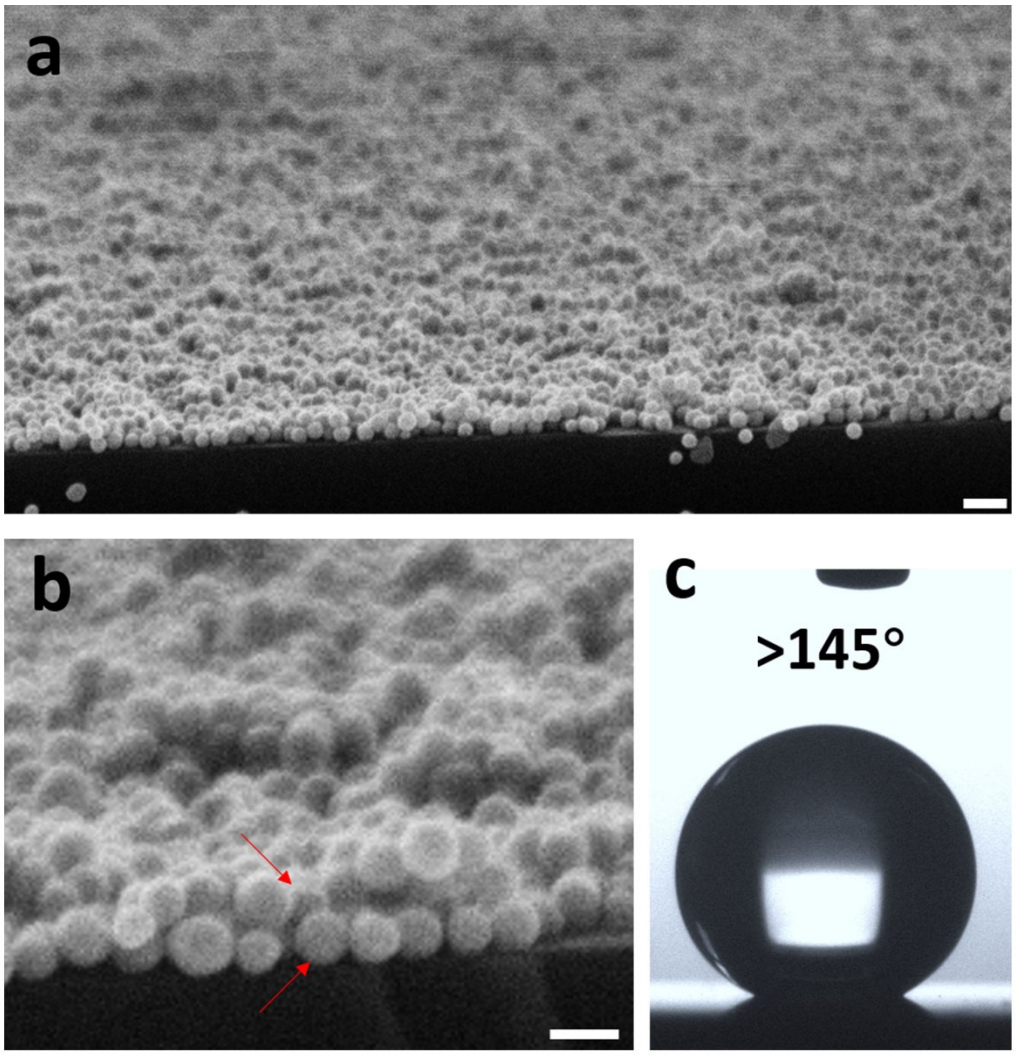

Figure S19. **SEM images and contact angle photograph of Au NPs multilayer structures.** SEM images (a-b) and contact angle photograph (c) of Au NPs multilayer structures acquired by repeated transferring Au NPs monolayer to the same substrate. The scale bar in d, e is 100 nm, 50 nm, respectively.

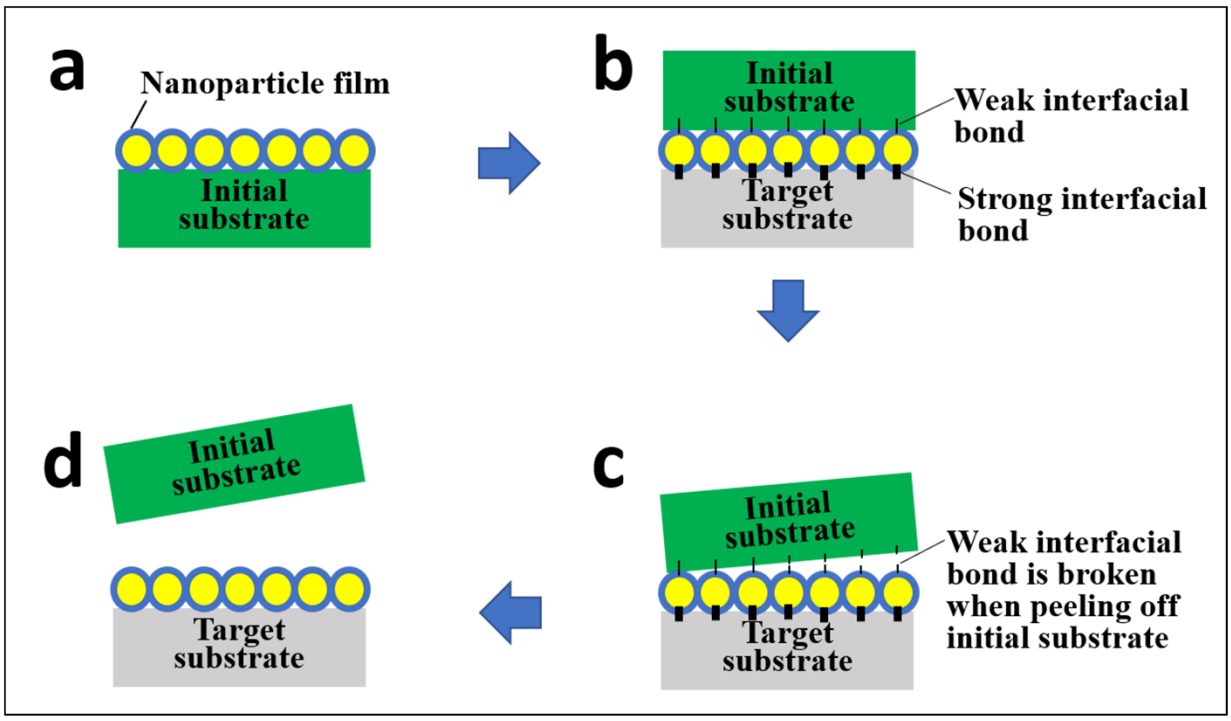

Figure S20. Schematic diagram of printing process and mechanism.

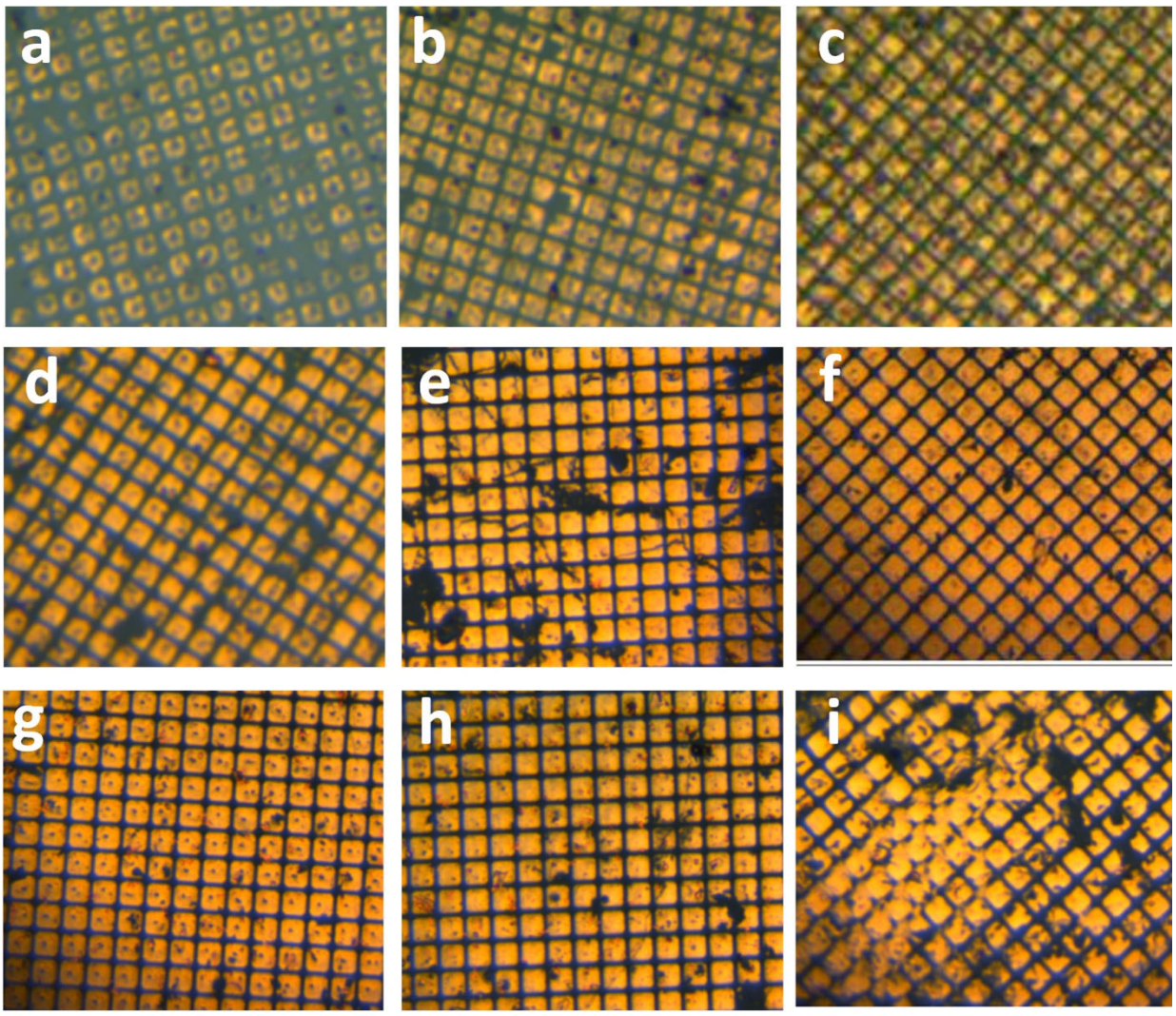

Figure S21. **Printing micropatterned Au NPs films on glass with different press pressure.** The press pressure in a-i is 0, 0.01, 0.02, 0.05. 0.1, 0.2, 0.5, 1, 2, 5 N, respectively.

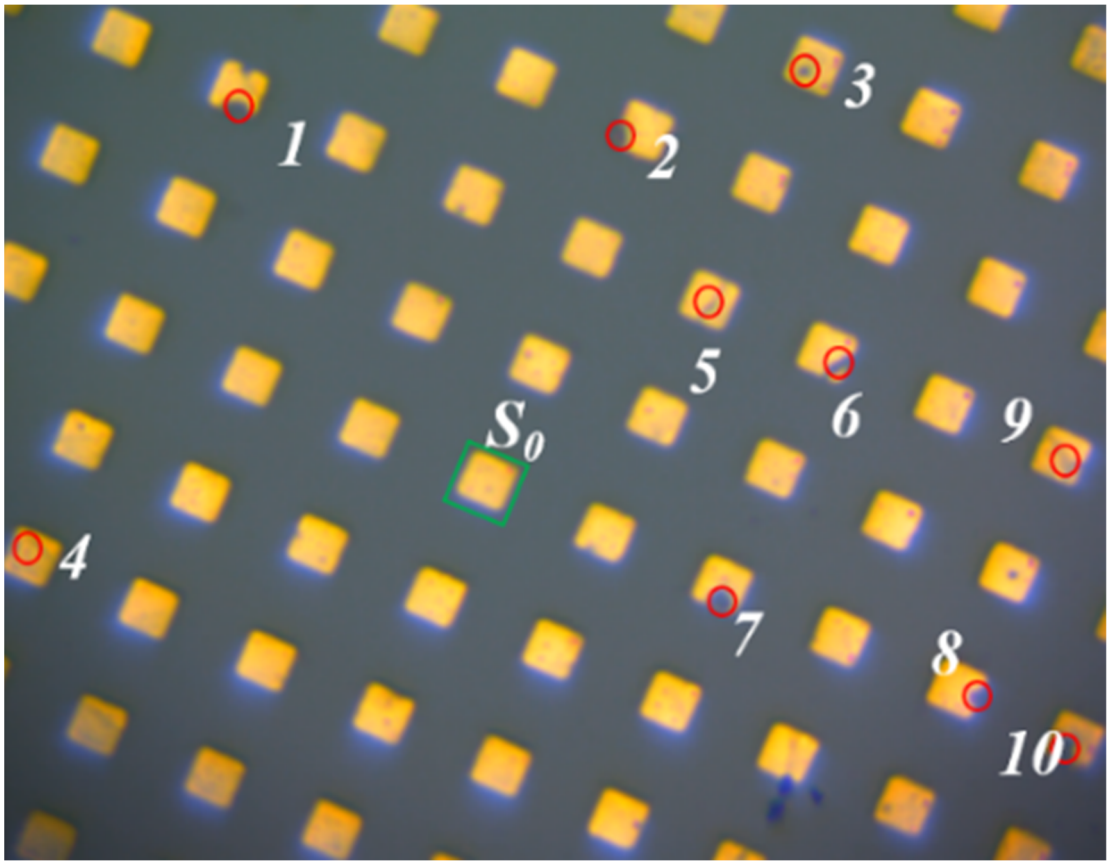

Figure S22. **The diagram for calculation of transferring efficiency.**

The transferring efficiency (η) was calculated as follows:

$$\eta\ (\%) = \frac{N \times S_0 - (S_1 + S_2 + S_3 + \cdots + S_n)}{N \times S_0} \times 100$$

In which S_0 is the unit area for definite topography, S_1, S_2, …, S_n is the defect area that failed to be transferred, N is the number of statistical units.

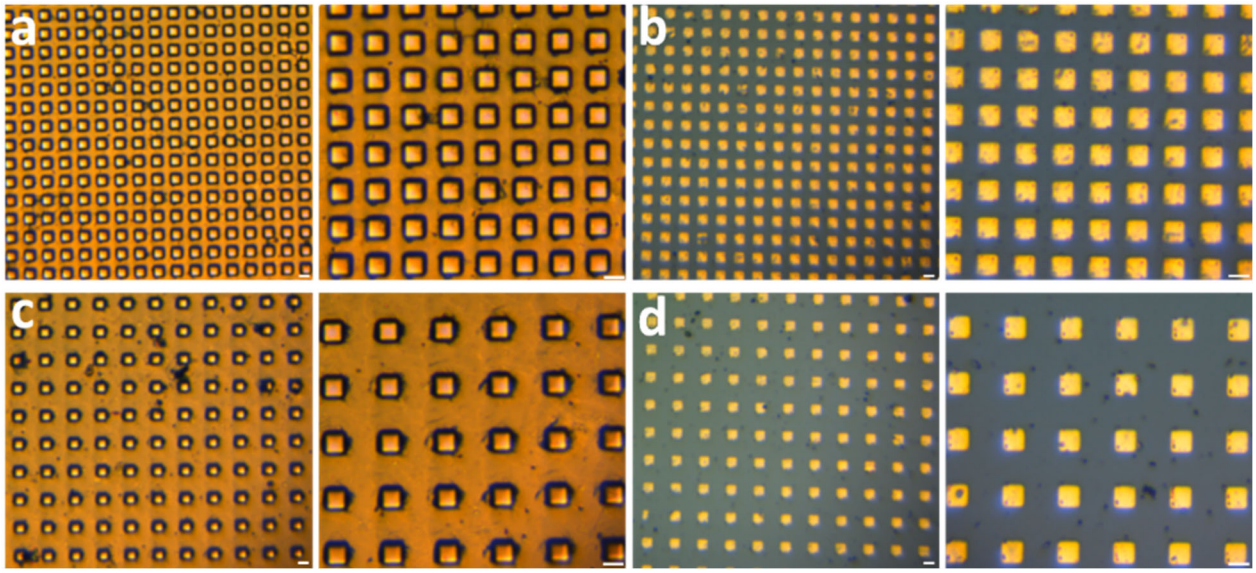

Figure S23. **Microphotographs of printing micropatterned Au NPs films with different spacing**: From PDMS (a, c) on glass (b, d). The scale bars are 10 μm.

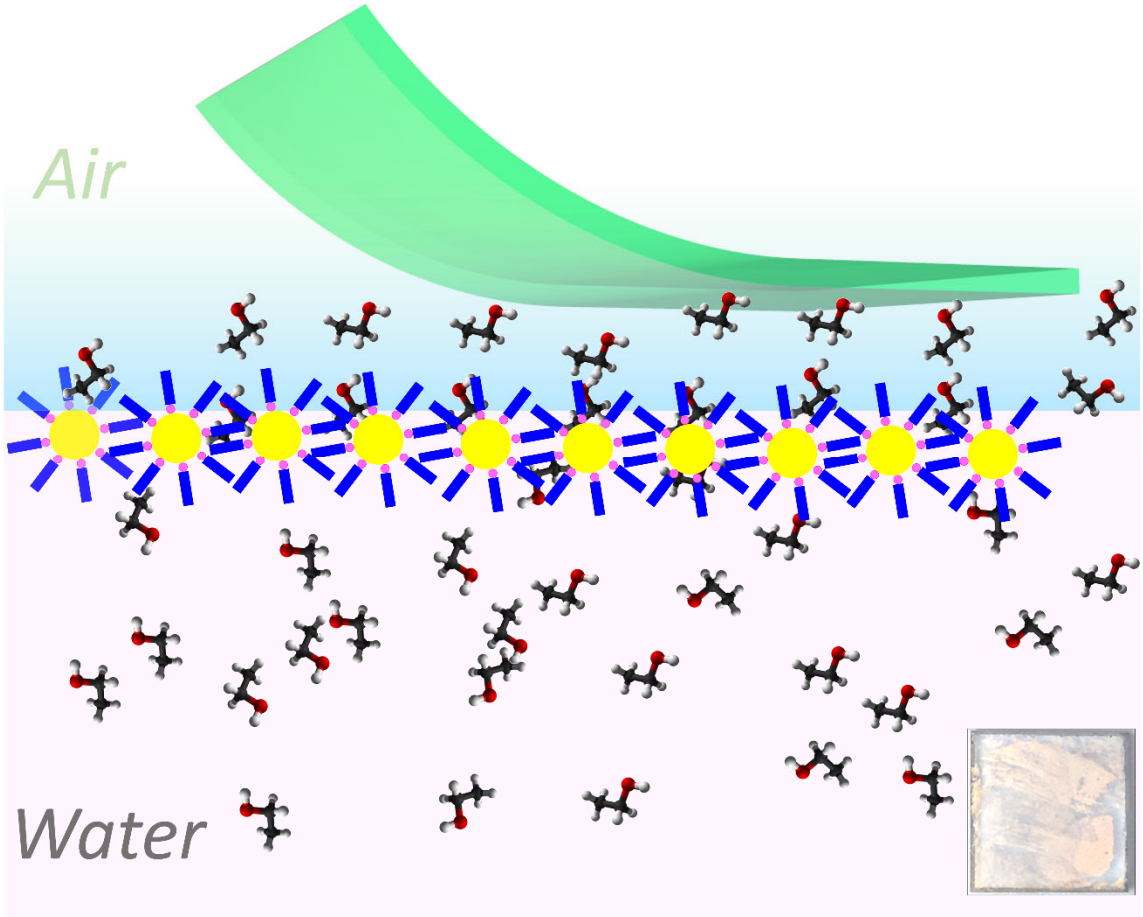

Figure S24. **The schematic diagram of ethanol bridged the Au NPs films with substrate and the photographs of Au NPs films on quartz glass after removing ethanol.** Photo credit: Liping Song, College of Material, Chemistry and Chemical Engineering, Hangzhou Normal University.

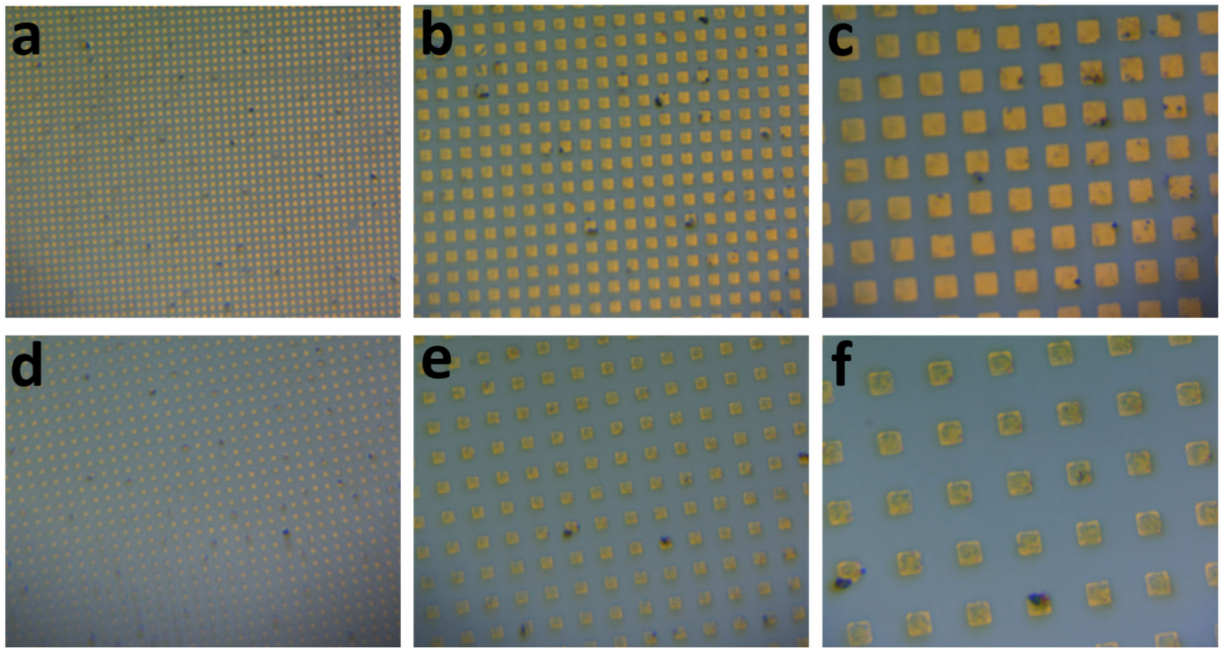

Figure S25. **Printing micropatterned Au NPs films on silicon wafer**: with (a-c)/without (b-d) plasma treatment.

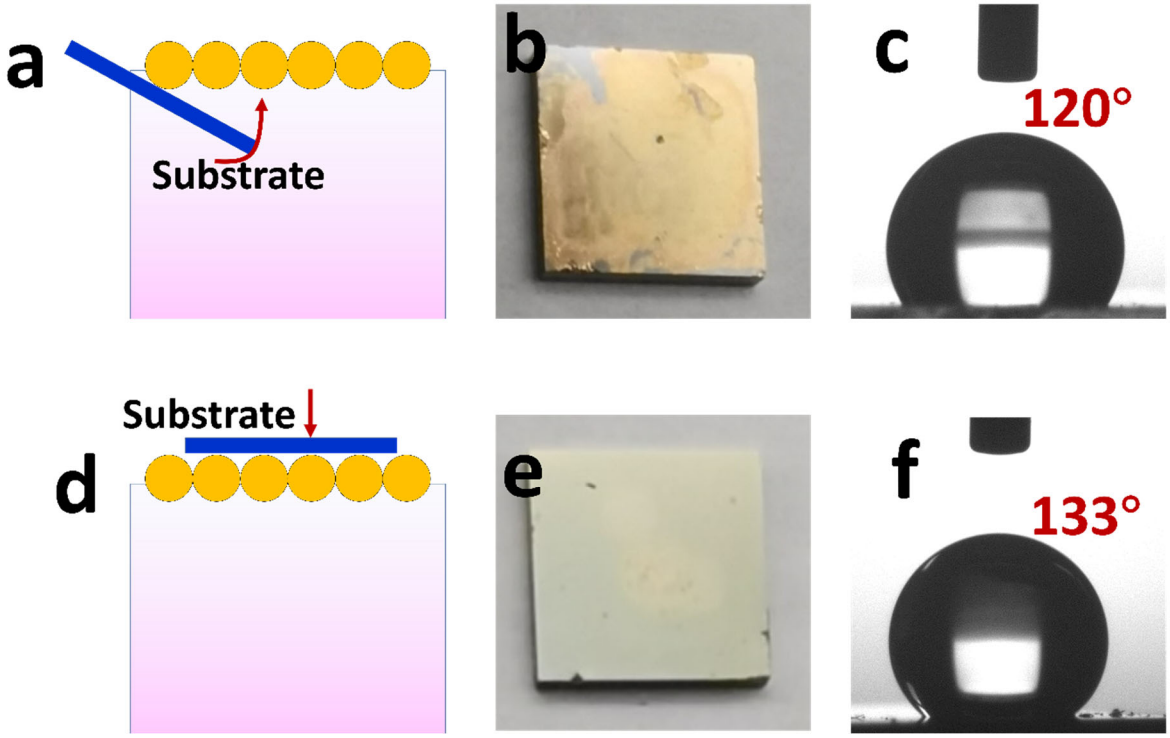

Figure S26. The Au NPs films obtained by transferring with different directions. Schematic diagram of different transferring direction for Au NPs monolayer films: (a) scooping up from water side of Au NPs film; (d) integrating to the air side of Au NPs film. The photographs obtained by transferring Au NPs with different direction: (b) scooping up from water side of Au NPs film; (c) integrating to the air side of Au NPs film. The contact angles of different surface of Au NPs films: (c) air side; (f) water side. Photo credit: Liping Song, College of Material, Chemistry and Chemical Engineering, Hangzhou Normal University.

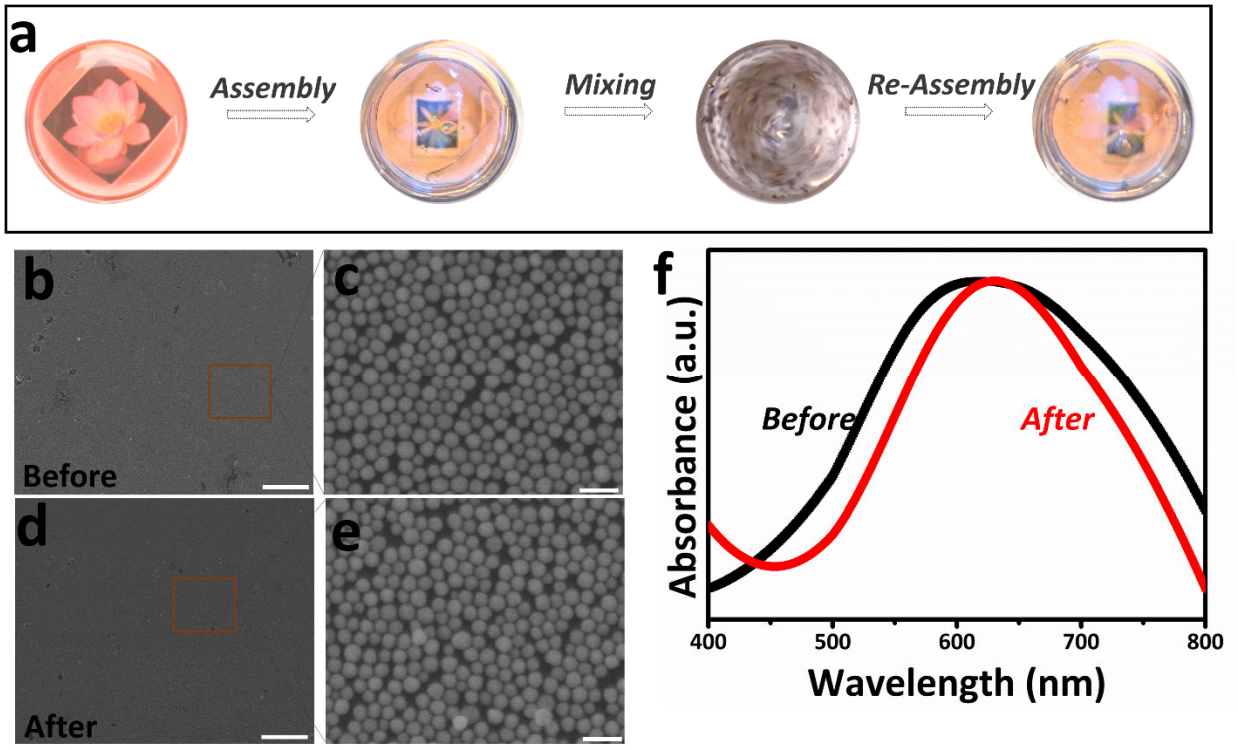

Figure S27. **The characterizations for the re-organization of Au NPs films at interface after mechanical disturbance.** (a) The images observed before, after and during violent mixing: the transferring from "Window" to "Mirror"; The SEM images of Au NPs assembled film before (b, c) and after (d, e) violent mixing. The scale bar in c, d is 5 μm, and in e, f is 50 nm; (f) the UV-vis spectra of Au NPs assembly before and after violent mixing. The violent mixing speed in all images is 1500 rpm. Photo credit: Liping Song, College of Material, Chemistry and Chemical Engineering, Hangzhou Normal University.

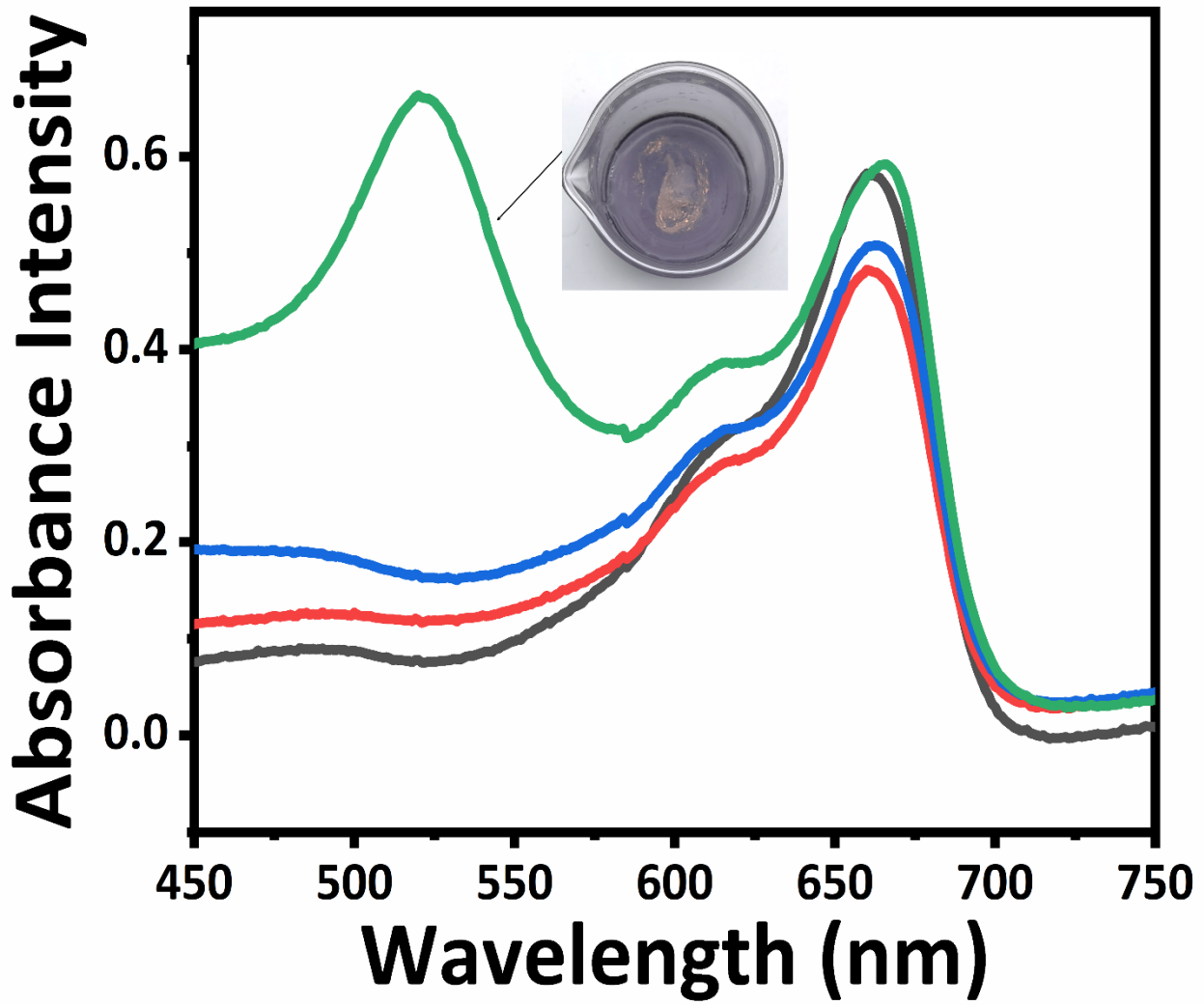

Figure S28. **The UV-vis spectra of MB aqueous solution before and after capturing by Au NPs films.** The UV-vis spectra of MB stock solution (black curve) and residual solution after with PFT-coated Au NPs films (red curve), without PFT coated Au NPs films (green curve) and without Au NPs films (blue curve) for MB capturing. The inset picture is the snapshot of Au NPs films formed without PFT after MB capturing. The amount of MB in all samples is 1 mL, 10^{-4} M. Photo credit: Liping Song, College of Material, Chemistry and Chemical Engineering, Hangzhou Normal University.

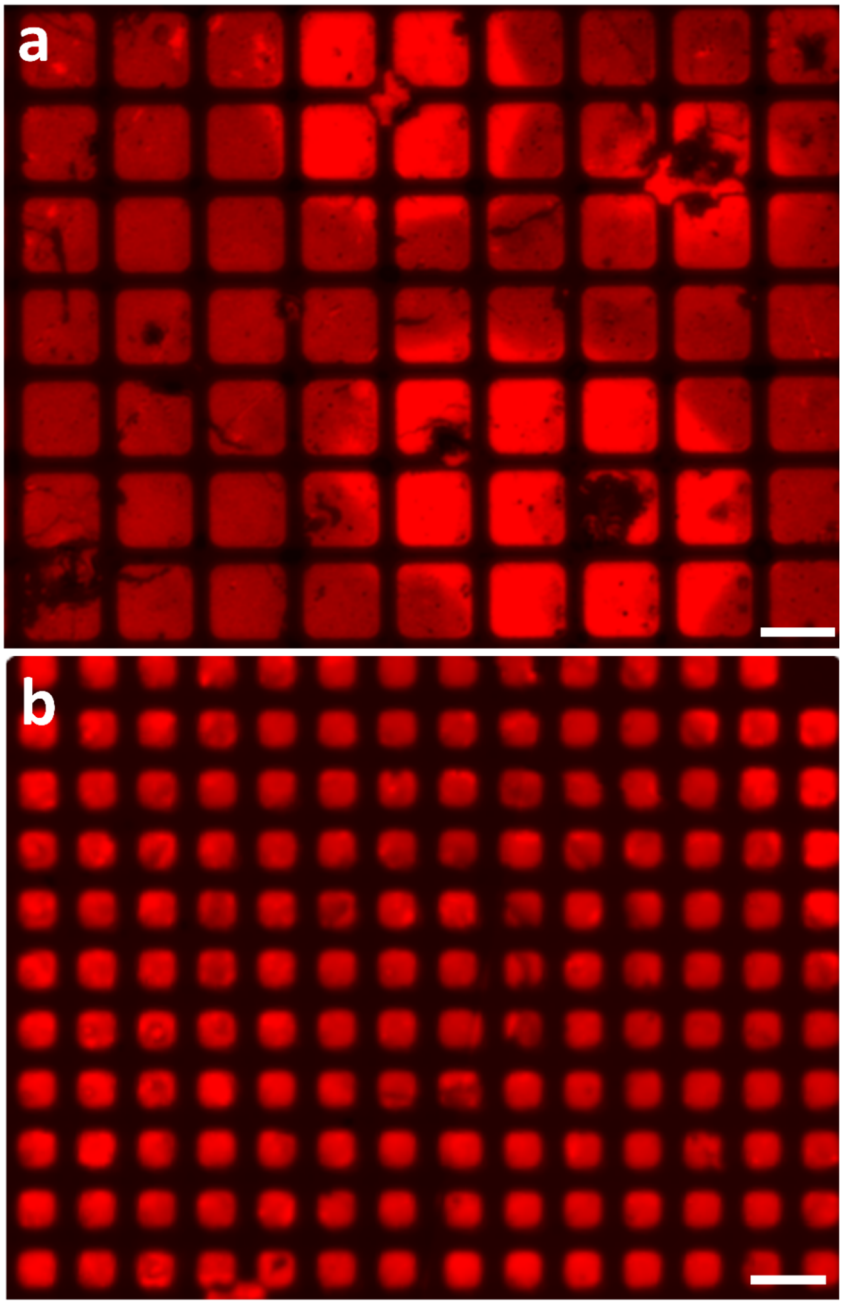

Figure S29. **The fluorescence images of self-assembled Au NPs-MB complexed micropatterns with different spacing**: Transferred from PDMS 2D on glass. λex = 644 nm. The scale bars are 10 μm.

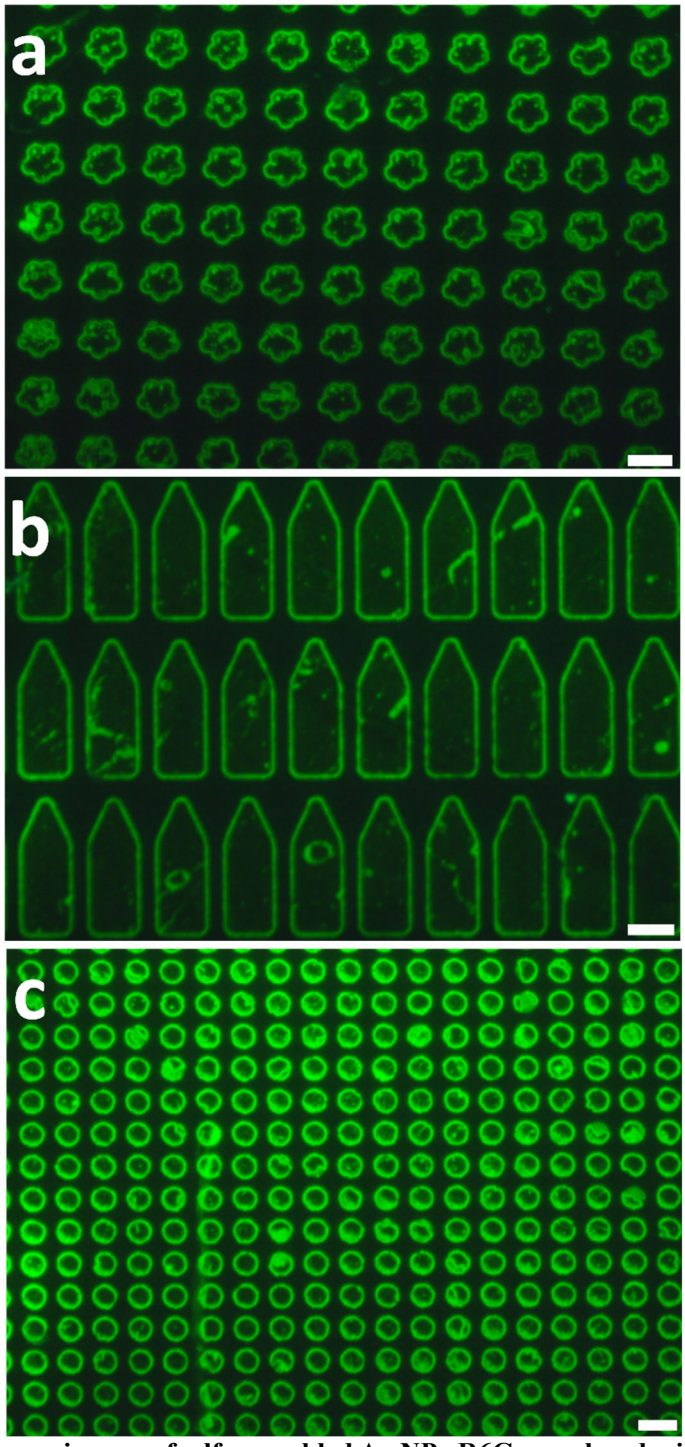

Figure S30. **The fluorescence images of self-assembled Au NPs-R6G complexed micropatterns**: Transferred from PDMS to glass. λex = 488 nm. The scale bars are 10 μm.

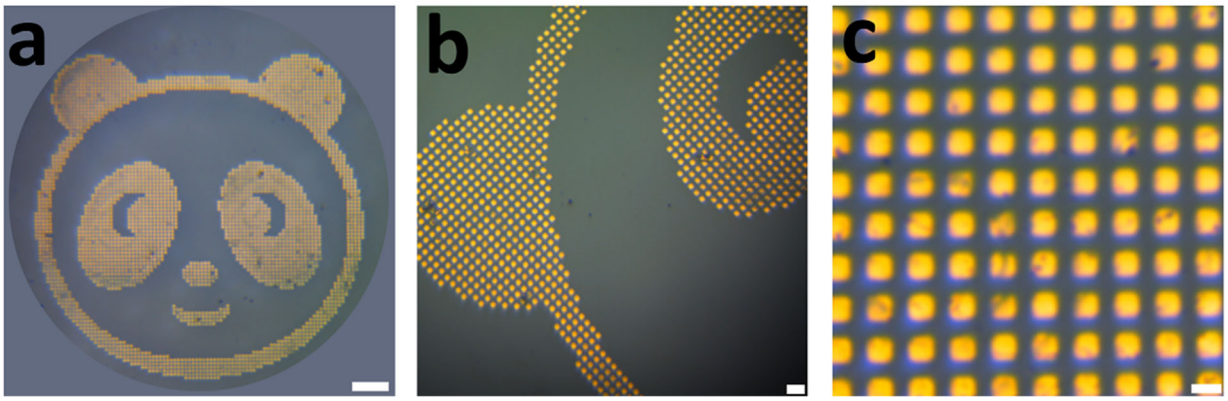

Figure S31. Microphotographs of "panda" micropattern of Au NPs-MB complexed films: From PDMS on glass. The scale bars in a, b, c is 100, 20 and 5 μm, respectively.

Table S1-S3

Table S1. **Interfacial assembly of Au NPs via different molecules assistance with discrepant surface energy.** Au NPs assembly via different molecules with sulphydryl group (including polyethyleneglycol (PEG), p-aminothiophenol (4-ATP), PFT as well as 1-dodecanethiol (DDT)) assistance with discrepant surface energy. The contact angle and surface energy of Au NPs films were tested on the contact angle meter. Photo credit: Liping Song, College of Material, Chemistry and Chemical Engineering, Hangzhou Normal University.

Molecular	PEG	4-ATP	PFT	DDT
Water Contact Angle				
Surface Energy (mN/m)	42.98	25.98	8.83	31.20
Assembly Photographs			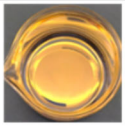	

Table S2. The comparison between PFT induced interfacial assembly with other similar interfacial approaches.

Interfacial assembly approaches	Ethanol Injecting Interfacial Assembly	**PFT Induced Interfacial Assembly**	Volatilizing Self-assembly on Solid Interface	Volatilizing Self-assembly on Liquid Interface	Promoter/Modifier Induced Assembly
Time	>20 min	**<5 s**	>24 h	>24 h	A few seconds/ or >3 h
Pretreatment of NPs	Washing	**Fresh NPs**	Surface Modification	Surface Modification	Surface Modification
Assembly Area	Several square centimeters	**Up to 96 cm^2 (the assembly area is determined by containers)**	≤ 1cm^2	Several square centimeters	≤ 1cm^2
Generalizability	Poorly	**Universal to noble NPs, oxides, polymers, QDs, carbon, etc.**	Almost impossible to be universal to other materials	Almost impossible to be universal to other materials	Poorly
NPs arrangement	Loose and inhomogeneous	**Density and uniform**	Density and inhomogeneous/ uniform	Density and uniform	Density and inhomogeneous
Ref.	15, 20		17, 57, 58	29, 59, 60	21, 31, 51

Table S3. The table of different materials for assembly with various functional groups.

Materials	Functional Groups
SC-Au NPs	$-COO^-$, -OH
CTAC-Au NPs	$(CH_3)_3N^+$
Ag NPs	-OH
SiO_2	$-NH_2$
QDs	-COOH
Au NPs@PANI	$-NH_2$
PS	=O, $-CH_3$

Movie S1. The display of instant assembly of Au NPs induced by PFT.

Movie S2. The mechanical stability display of assembled Au NPs films.

REFERENCES AND NOTES

1. S. Zhang, C. I. Pelligra, X. Feng, C. O. Osuji, Directed assembly of hybrid nanomaterials and nanocomposites. *Adv. Mater.* **30**, 1705794 (2018).

2. T. Das Gupta, L. Martin-Monier, W. Yan, A. Le Bris, T. Nguyen-Dang, A. G. Page, K.-T. Ho, F. Yesilköy, H. Altug, Y. Qu, F. Sorin, Self-assembly of nanostructured glass metasurfaces via templated fluid instabilities. *Nat. Nanotechnol.* **14**, 320–327 (2019).

3. Y. Liu, K. Du, I. Wathuthanthri, W. Xu, C. H. Choi, Freestanding photoresist film: A versatile template for three-dimensional micro- and nanofabrication. *Adv. Funct. Mater.* **30**, 2004129 (2020).

4. C. Jia, Z. Lin, Y. Huang, X. Duan, Nanowire electronics: From nanoscale to macroscale. *Chem. Rev.* **119**, 9074–9135 (2019).

5. J. Chang, J. Lee, A. Georgescu, D. Huh, T. Kang, Generalized on-demand production of nanoparticle monolayers on arbitrary solid surfaces via capillarity-mediated inverse transfer. *Nano Lett.* **19**, 2074–2083 (2019).

6. R. C. Webb, A. P. Bonifas, A. Behnaz, Y. Zhang, K. J. Yu, H. Cheng, M. Shi, Z. Bian, Z. Liu, Y.-S. Kim, W.-H. Yeo, J. S. Park, J. Song, Y. Li, Y. Huang, A. M. Gorbach, J. A. Rogers, Ultrathin conformal devices for precise and continuous thermal characterization of human skin. *Nat. Mater.* **12**, 938–944 (2013).

7. J. Kim, A. S. Campbell, B. E.-F. de Avila, J. Wang, Wearable biosensors for healthcare monitoring. *Nat. Biotechnol.* **37**, 389–406 (2019).

8. M. Su, F. Qin, Z. Zhang, B. Chen, Q. Pan, Z. Huang, Z. Cai, Z. Zhao, X. Hu, D. Derome, J. Carmeliet, Y. Song, Non-lithography hydrodynamic printing of micro/nanostructures on curved surfaces. *Angew. Chem. Int. Ed.* **59**, 14234–14240 (2020).

9. Z. Yan, T. Pan, M. Xue, C. Chen, Y. Cui, G. Yao, L. Huang, F. Liao, W. Jing, H. Zhang, M. Gao, D. Guo, Y. Xia, Y. Lin, Thermal release transfer printing for stretchable conformal bioelectronics. *Adv. Sci.* **4**, 1700251 (2017).

10. Y. Huang, H. Wu, L. Xiao, Y. Duan, H. Zhu, J. Bian, D. Yeab, Z. Yin, Assembly and applications of 3D conformal electronics on curvilinear surfaces. *Mater. Horiz.* **6**, 642–683 (2019).

11. M. D. Scanlon, E. Smirnov, T. J. Stockmann, P. Peljo, Gold nanofilms at liquid-liquid interfaces: An emerging platform for redox electrocatalysis, nanoplasmonic sensors, and electrovariable optics. *Chem. Rev.* **118**, 3722–3751 (2018).

12. W. Zhao, S. Xiao, Y. Zhang, D. Pan, J. Wen, X. Qian, D. Wang, H. Cao, W. He, M. Quan, Z. Yang, Binary "island" shaped arrays with high-density hot spots for surface-enhanced Raman scattering substrates. *Nanoscale* **10**, 14220–14229 (2018).

13. J. B. Lee, H. Walker, Y. Li, T. W. Nam, A. Rakovich, R. Sapienza, Y. S. Jung, Y. S. Nam, S. A. Maier, E. Cortés, Template dissolution interfacial patterning of single colloids for nanoelectrochemistry and nanosensing. *ACS Nano* **14**, 17693–17703 (2020).

14. T. R. Ray, J. Choi, A. J. Bandodkar, S. Krishnan, P. Gutruf, L. Tian, R. Ghaffari, J. A. Rogers, Bio-integrated wearable systems: A comprehensive review. *Chem. Rev.* **119**, 5461–5533 (2019).

15. Y. Shin, J. Song, D. Kim, T. Kang, Facile preparation of ultrasmall void metallic nanogap from self-assembled gold-silica core-shell nanoparticles monolayer via kinetic control. *Adv. Mater.* **27**, 4344–4350 (2015).

16. Y. Montelongo, D. Sikdar, Y. Ma, A. J. S. McIntosh, L. Velleman, A. R. Kucernak, J. B. Edel, A. A. Kornyshev, Electrotunable nanoplasmonic liquid mirror. *Nat. Mater.* **16**, 1127–1135 (2017).

17. J. Kim, X. Song, F. Ji, B. Luo, N. F. Ice, Q. Liu, Q. Zhang, Q. Che, Polymorphic assembly from beveled gold triangular nanoprisms. *Nano Lett.* **17**, 3270–3275 (2017).

18. Y. J. Li, W. J. Huang, S. G. Sun, A universal approach for the self-assembly of hydrophilic nanoparticles into ordered monolayer films at a toluene/water interface. *Angew. Chem. Int. Ed.* **45**, 2537–2539 (2006).

19. W. Zhao, Y. Zhang, J. Yang, J. Li, Y. Feng, M. Quan, Z. Yang, S. Xiao, Synergistic plasmon resonance coupling and light capture in ordered nanoarrays as ultrasensitive and reproducible SERS substrates. *Nanoscale* **12**, 18056–18066 (2020).

20. S. Si, W. Liang, Y. Sun, J. Huang, W. Ma, Z. Liang, Q. Bao, L. Jiang, Facile fabrication of high-density sub-1-nm gaps from Au nanoparticle monolayers as reproducible SERS substrates. *Adv. Funct. Mater.* **26**, 8137–8145 (2016).

21. Y. Liu, Y. Liu, P. Tao, W. Shang, C. Song, T. Deng, Vertical segregation in the self-assembly of nanoparticles at the liquid/air interface. *Nanoscale* **6**, 14662–14666 (2014).

22. H. Tian, H. Li, Y. Fang, Binary thiol-capped gold nanoparticle monolayer films for quantitative surface-enhanced Raman scattering analysis. *ACS Appl. Mater. Interfaces* **11**, 16207–16213 (2019).

23. B. P. Binks, Particles as surfactants-similarities and differences. *Curr. Opin. Colloid Interface Sci.* **7**, 21–41 (2002).

24. Z. Niu, J. He, T. P. Russell, Q. Wang, Synthesis of nano/microstructures at fluid interfaces. *Angew. Chem. Int. Ed.* **49**, 10052–10066 (2010).

25. J.-W. Hu, G.-B. Han, B. Ren, S.-G. Sun, Z.-Q. Tian, Theoretical consideration on preparing silver particle films by adsorbing nanoparticles from bulk colloids to an air-water interface. *Langmuir* **20**, 8831–8838 (2004).

26. R.-H. Yoon, D. H. Flinn, Y. I. Rabinovich, Hydrophobic interactions between dissimilar surfaces. *J. Colloid Interface Sci.* **185**, 363–370 (1997).

27. Q. Sun, B. Aguila, J. A. Perman, T. Butts, F.-S. Xiao, S. Ma, Integrating superwettability within covalent organic frameworks for functional coating. *Chem* **4**, 1726–1739 (2018).

28. P. Sun, L. M. Nowack, W. Bu, M. K. Bera, S. Griesemer, M. Reik, J. Portner, S. A. Rice, M. L. Schlossman, B. Lin, Free thiols regulate the interactions and self-assembly of thiol-passivated metal nanoparticles. *Nano Lett.* **21**, 1613–1619 (2021).

29. F. Schulz, O. Pavelka, F. Lehmkühler, F. Westermeier, Y. Okamura, N. S. Mueller, S. Reich, H. Lange, Structural order in plasmonic superlattices. *Nat. Commun.* **11**, 3821 (2020).

30. X. Lu, Y. Huang, B. Liu, L. Zhang, L. Song, J. Zhang, A. Zhang, T. Chen, Light-controlled shrinkage of large-area gold nanoparticle monolayer film for tunable SERS activity. *Chem. Mater.* **30**, 1989–1997 (2018).

31. Y. Xu, M. P. Konrad, W. W. Lee, Z. Ye, S. E. J. Bell, A method for promoting assembly of metallic and nonmetallic nanoparticles into interfacial monolayer films. *Nano Lett.* **16**, 5255–5260 (2016).

32. Y. Xu, F. Yu, M. Su, S. Du, H. Liu, Halide-assisted activation of atomic hydrogen for photoreduction on two-liquid interfacial plasmonic arrays. *Chem. Commun.* **55**, 1422–1425 (2019).

33. Y.-K. Park, S. Park, Directing close-packing of midnanosized gold nanoparticles at a water/hexane interface. *Chem. Mater.* **20**, 2388–2393 (2008).

34. M. J. Campolongo, S. J. Tian, D.-M. Smilgies, M. Zhao, Y. Chen, I. Xhangolli, W. Cheng, D. Luo, Crystalline gibbs monolayers of DNA-capped nanoparticles at the air–liquid interface. *ACS Nano* **5**, 7978–7985 (2011).

35. L. Wu, X. Wang, G. Wang, G. Chen, In situ x-ray scattering observation of two-dimensional interfacial colloidal crystallization. *Nat. Commun.* **9**, 1335 (2018).

36. V. H. Dalvi, P. J. Rossky, Molecular origins of fluorocarbon hydrophobicity. *Proc. Natl. Acad. Sci. U.S.A.* **107**, 13603–13607 (2010).

37. O. Bjorneholm, M. H. Hansen, A. Hodgson, L.-M. Liu, D. T. Limmer, A. Michaelides, P. Pedevilla, J. Rossmeisl, H. Shen, G. Tocci, E. Tyrode, M.-M. Walz, J. Werner, H. Bluhm, Water at interfaces. *Chem. Rev.* **116**, 7698–7726 (2016).

38. Y. Yu, Y. Hong, P. Gao, M. K. Nazeeruddin, Glutathione modified gold nanoparticles for sensitive colorimetric detection of Pb^{2+} ions in rainwater polluted by leaking perovskite solar cells. *Anal. Chem.* **88**, 12316–12322 (2016).

39. S. Yang, X. Dai, B. B. Stogin, T. S. Wong, Ultrasensitive surface-enhanced Raman scattering detection in common fluids. *Proc. Natl. Acad. Sci. U.S.A.* **113**, 268–273 (2016).

40. M. Kim, D. Ha, T. Kim, Cracking-assisted photolithography for mixed-scale patterning and nanofluidic applications. *Nat. Commun.* **6**, 6247 (2015).

41. T. W. Park, M. Byun, H. Jung, G. Lee, J. H. Park, H.-I. Jang, J. Lee, S. Kwon, S. Hong, J.-H. Lee, Y. S. Jung, K. H. Kim, W. I. Park, Thermally assisted nanotransfer printing with sub–20-nm resolution and 8-inch wafer scalability. *Sci. Adv.* **6**, eabb6462 (2020).

42. J. Feng, L. Peng, C. Wu, X. Sun, S. Hu, C. Lin, J. Dai, J. Yang, Y. Xie, Giant moisture responsiveness of VS_2 ultrathin nanosheets for novel touchless positioning interface. *Adv. Mater.* **24**, 1969–1974 (2012).

43. A. Carlson, A. M. Bowen, Y. Huang, R. G. Nuzzo, J. A. Rogers, Transfer printing techniques for materials assembly and micro/nanodevice fabrication. *Adv. Mater.* **24**, 5284–5318 (2012).

44. X. Feng, M. A. Meitl, A. M. Bowen, Y. Huang, R. G. Nuzzo, J. A. Rogers, Competing fracture in kinetically controlled transfer printing. *Langmuir* **23**, 12555–12560 (2007).

45. M. A. Meitl, Z.-T. Zhu, V. Kumar, K. J. Lee, X. Feng, Y. Y. Huang, I. Adesida, R. G. Nuzzo, J. A. Rogers, Transfer printing by kinetic control of adhesion to an elastomeric stamp. *Nat. Mater.* **5**, 33–38 (2005).

46. Z.-Y. Cao, W. Wang, K. Liao, X. Wang, J. Zhou, J. Ma, Catalytic enantioselective synthesis of cyclopropanes featuring vicinal all-carbon quaternary stereocenters with a CH_2F group;

study of the influence of C–F···H–N interactions on reactivity. *Org. Chem. Front.* **5**, 2960–2968 (2018).

47. J. S. Yu, Y. L. Liu, J. Tang, X. Wang, J. Zhou, Highly efficient “on water” catalyst-free nucleophilic addition reactions using difluoroenoxysilanes: Dramatic fluorine effects. *Angew. Chem. Int. Ed.* **53**, 9512–9516 (2014).

48. A. Dong, J. Chen, P. M. Vora, J. M. Kikkawa, C. B. Murray, Binary nanocrystal superlattice membranes self-assembled at the liquid-air interface. *Nature* **466**, 474–477 (2010).

49. X. Yu, L. Wu, D. Yang, M. Cao, X. Fan, H. Lin, Q. Zhong, Y. Xu, Q. Zhang, Hydrochromic $CsPbBr_3$ nanocrystals for anti-counterfeiting. *Angew. Chem. Int. Ed.* **59**, 14527–14532 (2020).

50. A. O. Larin, L. N. Dvoretckaia, A. M. Mozharov, I. S. Mukhin, A. B. Cherepakhin, I. I. Shishkin, E. I. Ageev, D. A. Zuev, Luminescent erbium-doped silicon thin films for advanced anti-counterfeit labels. *Adv. Mater.* **33**, e2005886 (2021).

51. L. Tian, M. Su, F. Yu, Y. Xu, X. Li, L. Li, H. Liu, W. Tan, Liquid-state quantitative SERS analyzer on self-ordered metal liquid-like plasmonic arrays. *Nat. Commun.* **9**, 3642 (2018).

52. N. G. Bastús, F. Merkoçi, J. Piella, V. Puntes, Synthesis of highly monodisperse citrate-stabilized silver nanoparticles of up to 200 nm: Kinetic control and catalytic properties. *Chem. Mater.* **26**, 2836–2846 (2014).

53. X. Ye, C. Zheng, J. Chen, Y. Gao, C. B. Murray, Using binary surfactant mixtures to simultaneously improve the dimensional tunability and monodispersity in the seeded growth of gold nanorods. *Nano Lett.* **13**, 765–771 (2013).

54. H. Lin, L. Song, Y. Huang, Q. Cheng, Y. Yang, Z. Guo, F. Su, T. Chen, Macroscopic Au@PANI core/shell nanoparticle superlattice monolayer film with dual-responsive plasmonic switches. *ACS Appl. Mater. Interfaces* **12**, 11296–11304 (2020).

55. L. Pan, S. Sun, L. Zhang, K. Jiang, H. Lin, Near-infrared emissive carbon dots for two-photon fluorescence bioimaging. *Nanoscale* **8**, 17350–17356 (2016).

56. T. Zhang, Q. Zhang, J. Ge, J. Goebl, M. Sun, Y. Yan, Y. Liu, C. Chang, J. Guo, Y. Yin, A self-templated route to hollow silica microspheres. *J. Phys. Chem. C* **113**, 3168–3175 (2009).

57. Q. Shi, D. E. Gómez, D. Dong, D. Sikdar, R. Fu, Y. Liu, Y. Zhao, D.-M. Smilgies, W. Cheng, 2D freestanding Janus gold nanocrystal superlattices. *Adv. Mater.* **31**, e1900989 (2019).

58. S. Pekdemir, I. Torun, M. Sakir, M. Ruzi, J. A. Rogers, M. S. Onses, Chemical funneling of colloidal gold nanoparticles on printed arrays of end-grafted polymers for plasmonic applications. *ACS Nano* **14**, 8276–8286 (2020).

59. T. Udayabhaskararao, T. Altantzis, L. Houben, M. Coronado-Puchau, J. Langer, R. Popovitz-Biro, L. M. Liz-Marzán, L. Vuković, P. Král, S. Bals, R. Klajn, Tunable porous nanoallotropes prepared by post-assembly etching of binary nanoparticle superlattices. *Science* **358**, 514–518 (2017).

60. K. Wang, H. Ling, Y. Bao, M. Yang, Y. Yang, M. Hussain, H. Wang, L. Zhang, L. Xie, M. Yi, W. Huang, X. Xie, J. Zhu, A centimeter-scale inorganic nanoparticle superlattice monolayer with non-close-packing and its high performance in memory devices. *Adv. Mater.* **30**, e1800595 (2018).

REFERENCES AND NOTES

1. S. Zhang, C. I. Pelligra, X. Feng, C. O. Osuji, Directed assembly of hybrid nanomaterials and nanocomposites. *Adv. Mater.* **30**, 1705794 (2018).

2. T. Das Gupta, L. Martin-Monier, W. Yan, A. Le Bris, T. Nguyen-Dang, A. G. Page, K.-T. Ho, F. Yesilköy, H. Altug, Y. Qu, F. Sorin, Self-assembly of nanostructured glass metasurfaces via templated fluid instabilities. *Nat. Nanotechnol.* **14**, 320–327 (2019).

3. Y. Liu, K. Du, I. Wathuthanthri, W. Xu, C. H. Choi, Freestanding photoresist film: A versatile template for three-dimensional micro- and nanofabrication. *Adv. Funct. Mater.* **30**, 2004129 (2020).

4. C. Jia, Z. Lin, Y. Huang, X. Duan, Nanowire electronics: From nanoscale to macroscale. *Chem. Rev.* **119**, 9074–9135 (2019).

5. J. Chang, J. Lee, A. Georgescu, D. Huh, T. Kang, Generalized on-demand production of nanoparticle monolayers on arbitrary solid surfaces via capillarity-mediated inverse transfer. *Nano Lett.* **19**, 2074–2083 (2019).

6. R. C. Webb, A. P. Bonifas, A. Behnaz, Y. Zhang, K. J. Yu, H. Cheng, M. Shi, Z. Bian, Z. Liu, Y.-S. Kim, W.-H. Yeo, J. S. Park, J. Song, Y. Li, Y. Huang, A. M. Gorbach, J. A. Rogers, Ultrathin conformal devices for precise and continuous thermal characterization of human skin. *Nat. Mater.* **12**, 938–944 (2013).

7. J. Kim, A. S. Campbell, B. E.-F. de Avila, J. Wang, Wearable biosensors for healthcare monitoring. *Nat. Biotechnol.* **37**, 389–406 (2019).

8. M. Su, F. Qin, Z. Zhang, B. Chen, Q. Pan, Z. Huang, Z. Cai, Z. Zhao, X. Hu, D. Derome, J. Carmeliet, Y. Song, Non-lithography hydrodynamic printing of micro/nanostructures on curved surfaces. *Angew. Chem. Int. Ed.* **59**, 14234–14240 (2020).

9. Z. Yan, T. Pan, M. Xue, C. Chen, Y. Cui, G. Yao, L. Huang, F. Liao, W. Jing, H. Zhang, M. Gao, D. Guo, Y. Xia, Y. Lin, Thermal release transfer printing for stretchable conformal bioelectronics. *Adv. Sci.* **4**, 1700251 (2017).

10. Y. Huang, H. Wu, L. Xiao, Y. Duan, H. Zhu, J. Bian, D. Yeab, Z. Yin, Assembly and applications of 3D conformal electronics on curvilinear surfaces. *Mater. Horiz.* **6**, 642–683 (2019).

11. M. D. Scanlon, E. Smirnov, T. J. Stockmann, P. Peljo, Gold nanofilms at liquid-liquid interfaces: An emerging platform for redox electrocatalysis, nanoplasmonic sensors, and electrovariable optics. *Chem. Rev.* **118**, 3722–3751 (2018).

12. W. Zhao, S. Xiao, Y. Zhang, D. Pan, J. Wen, X. Qian, D. Wang, H. Cao, W. He, M. Quan, Z. Yang, Binary "island" shaped arrays with high-density hot spots for surface-enhanced Raman scattering substrates. *Nanoscale* **10**, 14220–14229 (2018).

13. J. B. Lee, H. Walker, Y. Li, T. W. Nam, A. Rakovich, R. Sapienza, Y. S. Jung, Y. S. Nam, S. A. Maier, E. Cortés, Template dissolution interfacial patterning of single colloids for nanoelectrochemistry and nanosensing. *ACS Nano* **14**, 17693–17703 (2020).

14. T. R. Ray, J. Choi, A. J. Bandodkar, S. Krishnan, P. Gutruf, L. Tian, R. Ghaffari, J. A. Rogers, Bio-integrated wearable systems: A comprehensive review. *Chem. Rev.* **119**, 5461–5533 (2019).

15. Y. Shin, J. Song, D. Kim, T. Kang, Facile preparation of ultrasmall void metallic nanogap from self-assembled gold-silica core-shell nanoparticles monolayer via kinetic control. *Adv. Mater.* **27**, 4344–4350 (2015).

16. Y. Montelongo, D. Sikdar, Y. Ma, A. J. S. McIntosh, L. Velleman, A. R. Kucernak, J. B. Edel, A. A. Kornyshev, Electrotunable nanoplasmonic liquid mirror. *Nat. Mater.* **16**, 1127–1135 (2017).

17. J. Kim, X. Song, F. Ji, B. Luo, N. F. Ice, Q. Liu, Q. Zhang, Q. Che, Polymorphic assembly from beveled gold triangular nanoprisms. *Nano Lett.* **17**, 3270–3275 (2017).

18. Y. J. Li, W. J. Huang, S. G. Sun, A universal approach for the self-assembly of hydrophilic nanoparticles into ordered monolayer films at a toluene/water interface. *Angew. Chem. Int. Ed.* **45**, 2537–2539 (2006).

19. W. Zhao, Y. Zhang, J. Yang, J. Li, Y. Feng, M. Quan, Z. Yang, S. Xiao, Synergistic plasmon resonance coupling and light capture in ordered nanoarrays as ultrasensitive and reproducible SERS substrates. *Nanoscale* **12**, 18056–18066 (2020).

20. S. Si, W. Liang, Y. Sun, J. Huang, W. Ma, Z. Liang, Q. Bao, L. Jiang, Facile fabrication of high-density sub-1-nm gaps from Au nanoparticle monolayers as reproducible SERS substrates. *Adv. Funct. Mater.* **26**, 8137–8145 (2016).

21. Y. Liu, Y. Liu, P. Tao, W. Shang, C. Song, T. Deng, Vertical segregation in the self-assembly of nanoparticles at the liquid/air interface. *Nanoscale* **6**, 14662–14666 (2014).

22. H. Tian, H. Li, Y. Fang, Binary thiol-capped gold nanoparticle monolayer films for quantitative surface-enhanced Raman scattering analysis. *ACS Appl. Mater. Interfaces* **11**, 16207–16213 (2019).

23. B. P. Binks, Particles as surfactants-similarities and differences. *Curr. Opin. Colloid Interface Sci.* **7**, 21–41 (2002).

24. Z. Niu, J. He, T. P. Russell, Q. Wang, Synthesis of nano/microstructures at fluid interfaces. *Angew. Chem. Int. Ed.* **49**, 10052–10066 (2010).

25. J.-W. Hu, G.-B. Han, B. Ren, S.-G. Sun, Z.-Q. Tian, Theoretical consideration on preparing silver particle films by adsorbing nanoparticles from bulk colloids to an air-water interface. *Langmuir* **20**, 8831–8838 (2004).

26. R.-H. Yoon, D. H. Flinn, Y. I. Rabinovich, Hydrophobic interactions between dissimilar surfaces. *J. Colloid Interface Sci.* **185**, 363–370 (1997).

27. Q. Sun, B. Aguila, J. A. Perman, T. Butts, F.-S. Xiao, S. Ma, Integrating superwettability within covalent organic frameworks for functional coating. *Chem* **4**, 1726–1739 (2018).

28. P. Sun, L. M. Nowack, W. Bu, M. K. Bera, S. Griesemer, M. Reik, J. Portner, S. A. Rice, M. L. Schlossman, B. Lin, Free thiols regulate the interactions and self-assembly of thiol-passivated metal nanoparticles. *Nano Lett.* **21**, 1613–1619 (2021).

29. F. Schulz, O. Pavelka, F. Lehmkühler, F. Westermeier, Y. Okamura, N. S. Mueller, S. Reich, H. Lange, Structural order in plasmonic superlattices. *Nat. Commun.* **11**, 3821 (2020).

30. X. Lu, Y. Huang, B. Liu, L. Zhang, L. Song, J. Zhang, A. Zhang, T. Chen, Light-controlled shrinkage of large-area gold nanoparticle monolayer film for tunable SERS activity. *Chem. Mater.* **30**, 1989–1997 (2018).

31. Y. Xu, M. P. Konrad, W. W. Lee, Z. Ye, S. E. J. Bell, A method for promoting assembly of metallic and nonmetallic nanoparticles into interfacial monolayer films. *Nano Lett.* **16**, 5255–5260 (2016).

32. Y. Xu, F. Yu, M. Su, S. Du, H. Liu, Halide-assisted activation of atomic hydrogen for photoreduction on two-liquid interfacial plasmonic arrays. *Chem. Commun.* **55**, 1422–1425 (2019).

33. Y.-K. Park, S. Park, Directing close-packing of midnanosized gold nanoparticles at a water/hexane interface. *Chem. Mater.* **20**, 2388–2393 (2008).

34. M. J. Campolongo, S. J. Tian, D.-M. Smilgies, M. Zhao, Y. Chen, I. Xhangolli, W. Cheng, D. Luo, Crystalline gibbs monolayers of DNA-capped nanoparticles at the air–liquid interface. *ACS Nano* **5**, 7978–7985 (2011).

35. L. Wu, X. Wang, G. Wang, G. Chen, In situ x-ray scattering observation of two-dimensional interfacial colloidal crystallization. *Nat. Commun.* **9**, 1335 (2018).

36. V. H. Dalvi, P. J. Rossky, Molecular origins of fluorocarbon hydrophobicity. *Proc. Natl. Acad. Sci. U.S.A.* **107**, 13603–13607 (2010).

37. O. Bjorneholm, M. H. Hansen, A. Hodgson, L.-M. Liu, D. T. Limmer, A. Michaelides, P. Pedevilla, J. Rossmeisl, H. Shen, G. Tocci, E. Tyrode, M.-M. Walz, J. Werner, H. Bluhm, Water at interfaces. *Chem. Rev.* **116**, 7698–7726 (2016).

38. Y. Yu, Y. Hong, P. Gao, M. K. Nazeeruddin, Glutathione modified gold nanoparticles for sensitive colorimetric detection of Pb^{2+} ions in rainwater polluted by leaking perovskite solar cells. *Anal. Chem.* **88**, 12316–12322 (2016).

39. S. Yang, X. Dai, B. B. Stogin, T. S. Wong, Ultrasensitive surface-enhanced Raman scattering detection in common fluids. *Proc. Natl. Acad. Sci. U.S.A.* **113**, 268–273 (2016).

40. M. Kim, D. Ha, T. Kim, Cracking-assisted photolithography for mixed-scale patterning and nanofluidic applications. *Nat. Commun.* **6**, 6247 (2015).

41. T. W. Park, M. Byun, H. Jung, G. Lee, J. H. Park, H.-I. Jang, J. Lee, S. Kwon, S. Hong, J.-H. Lee, Y. S. Jung, K. H. Kim, W. I. Park, Thermally assisted nanotransfer printing with sub–20-nm resolution and 8-inch wafer scalability. *Sci. Adv.* **6**, eabb6462 (2020).

42. J. Feng, L. Peng, C. Wu, X. Sun, S. Hu, C. Lin, J. Dai, J. Yang, Y. Xie, Giant moisture responsiveness of VS_2 ultrathin nanosheets for novel touchless positioning interface. *Adv. Mater.* **24**, 1969–1974 (2012).

43. A. Carlson, A. M. Bowen, Y. Huang, R. G. Nuzzo, J. A. Rogers, Transfer printing techniques for materials assembly and micro/nanodevice fabrication. *Adv. Mater.* **24**, 5284–5318 (2012).

44. X. Feng, M. A. Meitl, A. M. Bowen, Y. Huang, R. G. Nuzzo, J. A. Rogers, Competing fracture in kinetically controlled transfer printing. *Langmuir* **23**, 12555–12560 (2007).

45. M. A. Meitl, Z.-T. Zhu, V. Kumar, K. J. Lee, X. Feng, Y. Y. Huang, I. Adesida, R. G. Nuzzo, J. A. Rogers, Transfer printing by kinetic control of adhesion to an elastomeric stamp. *Nat. Mater.* **5**, 33–38 (2005).

46. Z.-Y. Cao, W. Wang, K. Liao, X. Wang, J. Zhou, J. Ma, Catalytic enantioselective synthesis of cyclopropanes featuring vicinal all-carbon quaternary stereocenters with a CH_2F group;

study of the influence of C–F···H–N interactions on reactivity. *Org. Chem. Front.* **5**, 2960–2968 (2018).

47. J. S. Yu, Y. L. Liu, J. Tang, X. Wang, J. Zhou, Highly efficient "on water" catalyst-free nucleophilic addition reactions using difluoroenoxysilanes: Dramatic fluorine effects. *Angew. Chem. Int. Ed.* **53**, 9512–9516 (2014).

48. A. Dong, J. Chen, P. M. Vora, J. M. Kikkawa, C. B. Murray, Binary nanocrystal superlattice membranes self-assembled at the liquid-air interface. *Nature* **466**, 474–477 (2010).

49. X. Yu, L. Wu, D. Yang, M. Cao, X. Fan, H. Lin, Q. Zhong, Y. Xu, Q. Zhang, Hydrochromic $CsPbBr_3$ nanocrystals for anti-counterfeiting. *Angew. Chem. Int. Ed.* **59**, 14527–14532 (2020).

50. A. O. Larin, L. N. Dvoretckaia, A. M. Mozharov, I. S. Mukhin, A. B. Cherepakhin, I. I. Shishkin, E. I. Ageev, D. A. Zuev, Luminescent erbium-doped silicon thin films for advanced anti-counterfeit labels. *Adv. Mater.* **33**, e2005886 (2021).

51. L. Tian, M. Su, F. Yu, Y. Xu, X. Li, L. Li, H. Liu, W. Tan, Liquid-state quantitative SERS analyzer on self-ordered metal liquid-like plasmonic arrays. *Nat. Commun.* **9**, 3642 (2018).

52. N. G. Bastús, F. Merkoçi, J. Piella, V. Puntes, Synthesis of highly monodisperse citrate-stabilized silver nanoparticles of up to 200 nm: Kinetic control and catalytic properties. *Chem. Mater.* **26**, 2836–2846 (2014).

53. X. Ye, C. Zheng, J. Chen, Y. Gao, C. B. Murray, Using binary surfactant mixtures to simultaneously improve the dimensional tunability and monodispersity in the seeded growth of gold nanorods. *Nano Lett.* **13**, 765–771 (2013).

54. H. Lin, L. Song, Y. Huang, Q. Cheng, Y. Yang, Z. Guo, F. Su, T. Chen, Macroscopic Au@PANI core/shell nanoparticle superlattice monolayer film with dual-responsive plasmonic switches. *ACS Appl. Mater. Interfaces* **12**, 11296–11304 (2020).

55. L. Pan, S. Sun, L. Zhang, K. Jiang, H. Lin, Near-infrared emissive carbon dots for two-photon fluorescence bioimaging. *Nanoscale* **8**, 17350–17356 (2016).

56. T. Zhang, Q. Zhang, J. Ge, J. Goebl, M. Sun, Y. Yan, Y. Liu, C. Chang, J. Guo, Y. Yin, A self-templated route to hollow silica microspheres. *J. Phys. Chem. C* **113**, 3168–3175 (2009).

57. Q. Shi, D. E. Gómez, D. Dong, D. Sikdar, R. Fu, Y. Liu, Y. Zhao, D.-M. Smilgies, W. Cheng, 2D freestanding Janus gold nanocrystal superlattices. *Adv. Mater.* **31**, e1900989 (2019).

58. S. Pekdemir, I. Torun, M. Sakir, M. Ruzi, J. A. Rogers, M. S. Onses, Chemical funneling of colloidal gold nanoparticles on printed arrays of end-grafted polymers for plasmonic applications. *ACS Nano* **14**, 8276–8286 (2020).

59. T. Udayabhaskararao, T. Altantzis, L. Houben, M. Coronado-Puchau, J. Langer, R. Popovitz-Biro, L. M. Liz-Marzán, L. Vuković, P. Král, S. Bals, R. Klajn, Tunable porous nanoallotropes prepared by post-assembly etching of binary nanoparticle superlattices. *Science* **358**, 514–518 (2017).

60. K. Wang, H. Ling, Y. Bao, M. Yang, Y. Yang, M. Hussain, H. Wang, L. Zhang, L. Xie, M. Yi, W. Huang, X. Xie, J. Zhu, A centimeter-scale inorganic nanoparticle superlattice monolayer with non-close-packing and its high performance in memory devices. *Adv. Mater.* **30**, e1800595 (2018).